Synthesis and Structure–Property Relationships of Cryogels

Oguz Okay and Vladimir I. Lozinsky

Contents

O. Okay (✉)
Department of Chemistry, Istanbul Technical University, 34469 Istanbul, Turkey
e-mail: okayo@itu.edu.tr

V.I. Lozinsky
Laboratory for Cryochemistry of (Bio)Polymers, A.N. Nesmeyanov Institute of Organoelement Compounds, Russian Academy of Sciences, Vavilov Street 28, 119991 Moscow, Russian Federation
e-mail: loz@ineos.ac.ru

O. Okay (ed.), *Polymeric Cryogels*, Advances in Polymer Science 263,
DOI 10.1007/978-3-319-05846-7_3,

Abstract Polymeric gels belong to the most important class of functional polymers in modern biotechnology. They are useful materials for drug delivery systems, artificial organs, separation operations in biotechnology, processing of agricultural products, on–off switches, sensors, and actuators. Despite this fact and considerable research in this field, the design and control of gel-based devices still present some problems due to the their poor mechanical performance and slow rate of response to external stimuli. Cryogelation techniques discovered more than 30 years ago overcome these limitations by producing macroporous gels with high toughness and superfast responsivity. This chapter discusses how and why the properties of gels significantly alter upon transition from homogeneous gelation to a cryogelation regime. The formation and structure–property relationships of cryogels starting from monovinyl–divinyl monomers, as well as from linear polymer chains, are reviewed using examples from the recent literature. Some novel cryogels with a wide range of tunable properties and their applications are also presented in detail. These include DNA cryogels for the removal of carcinogens from aqueous environments, silk fibroin cryogels as mechanically strong scaffolds for bone tissue engineering applications, poly(acrylic acid) cryogels as self-oscillation systems, and rubber cryogels as reusable oil sorbent for the removal of oil spill from seawater.

Keywords Cryogels • Porosity formation • Gelation • Elasticity • Swelling

Abbreviations

α	Dissociation degree
χ	Polymer–solvent interaction parameter
λ	Deformation ratio
ν_e	Effective crosslink density
σ	Nominal stress
σ_{comp}	Compressive stress
σ_p	Critical stress corresponding to the plateau regime
AAc	Acrylic acid
AAm	Acrylamide
AMPS	2-Acrylamido-2-methylpropane sulfonic acid sodium salt
APS	Ammonium persulfate
BAAm	*N*,*N*-methylene(bis)acrylamide
BDDE	1,4-Butanediol diglycidyl ether
C	Monomer concentration in the unfrozen zones
CBR	*cis*-Polybutadiene
C_o	Initial concentration of the monomeric or the polymeric precursors
C_R	Rubber concentration
C_{SF}	Fibroin concentration
DMA	*N*,*N*-Dimethylacrylamide

DMSO	Dimethyl sulfoxide
DNA	Deoxyribonucleic acid
E	Young's modulus
EGDE	Ethylene glycol diglycidyl ether
EtBr	Ethidium bromide
f	Effective charge density
G	Shear modulus
HEMA	2-Hydroxyethyl methacrylate
k	Reduced flow rate
m_{rel}	Normalized gel mass with respect to its equilibrium swollen mass
NIPA	*N*-Isopropylacrylamide
P	Total porosity or the volume fraction of frozen solvent in the reaction system
PAAc	Poly(acrylic acid)
PAAm	Polyacrylamide
PAMPS	Poly(AMPS)
PDMA	Poly(DMA)
PIB	Butyl rubber, a linear polyisobutylene containing small amounts of internal unsaturated groups (isoprene units)
PMAAc	Poly(methacrylic acid)
PNIPA	Poly(NIPA)
P_s	Swollen state porosity
PSA	Poly(SA)
PVA	Poly(vinyl alcohol)
q_v	Equilibrium volume swelling ratio (with respect to dry state)
q_w	Equilibrium weight swelling ratio (with respect to dry state)
SA	Sodium acrylate
SBR	Styrene-butadiene rubber
SEM	Scanning electron microscopy
TEMED	*N*,*N*,*N*′,*N*′-Tetramethylethylenediamine
T_{prep}	Cryogelation temperature
V_1	Molar volume of solvent
V_{eq}	Volume swelling ratio with respect to the after preparation state of gels
V_p	Total volume of open pores

1 Introduction

Polymeric gels are crosslinked polymers swollen in a liquid. The polymer serves as a matrix to hold the liquid together, while the liquid inside the gel allows free diffusion of some solute molecules. Polymeric gels can be prepared from either monomeric or polymeric precursors dissolved in a solvent. However, the most commonly used method is the free-radical crosslinking copolymerization of a monovinyl monomer with a divinyl monomer (crosslinker) in solution. In the

case of hydrophilic gels, called hydrogels, an ionic comonomer is also included in the monomer mixture to increase the swelling capacity in aqueous environment. The desired property of gels, such as the swelling capacity, the modulus of elasticity, and the degree of heterogeneity, is obtained by adjusting the concentration as well as the composition of the reaction constituents [1]. Ionic hydrogels swell up to 1,000 times their dry volume when in contact with water. They also exhibit drastic volume changes in response to specific external stimuli such as temperature, solvent quality, pH, electric field, etc [2]. Depending on the design of the hydrogel matrices, this volume change may occur continuously over a range of stimulus level, or discontinuously at a critical stimulus level. These properties of hydrogels and their similarities to biological systems have received considerable interest over the last three decades. Today, these soft and smart materials belong to the most important class of functional polymers in modern biotechnology [3]. They are useful materials for drug delivery systems, artificial organs, separation operations in biotechnology, processing of agricultural products, on–off switches, sensors, and actuators [1, 4].

Despite this fact and considerable research in this field, the design and control of gel-based devices still present some problems because a number of network properties are inversely coupled. For example, decreasing the degree of crosslinking of gels in order to increase their mesh size results in their accelerated degradation. Further, loosely crosslinked gels are fragile materials when handled in the swollen state; typically, they rupture at very low strains due to the lack of an efficient energy dissipation mechanism in the gel network. Moreover, the response rate of gels to external stimuli is not as fast as required in many application areas. This is due to the fact that the kinetics of the gel volume change involves absorbing or desorbing solvent by the polymer network, which is a diffusive process. This process is slow, and even slower near the critical point [5]. Hence, design of gels with a good mechanical performance together with a fast response rate is crucially important in many existing and potential application areas of soft materials.

A number of techniques for toughening of gels have recently been proposed, including double network gels [6], topological gels [7], gels formed by hydrophobic associations [8], gels made by mobile crosslinkers such as clay nanoparticles (nanocomposite hydrogels) [9], and microsphere composite hydrogels [10]. Although these techniques create energy dissipation mechanisms to slow crack propagation and, thus, improve the mechanical properties of gels, they exhibit a slow response rate to external stimuli. In order to achieve rapid changes in the gel volume, a common strategy is to create an interconnected pore structure inside the gel network [11]. For a polymer network having an interconnected pore structure, absorption or desorption of solvent occurs through the pores by convection, which is much faster than the diffusion process that dominates the nonporous polymer networks.[1] The basic technique for obtaining polymer gels with a macroporous

[1] In the early works, the space between the network chains in a swollen homogeneous gel was defined as “porosity” or “molecular porosity.” However, this term is clearly misleading because

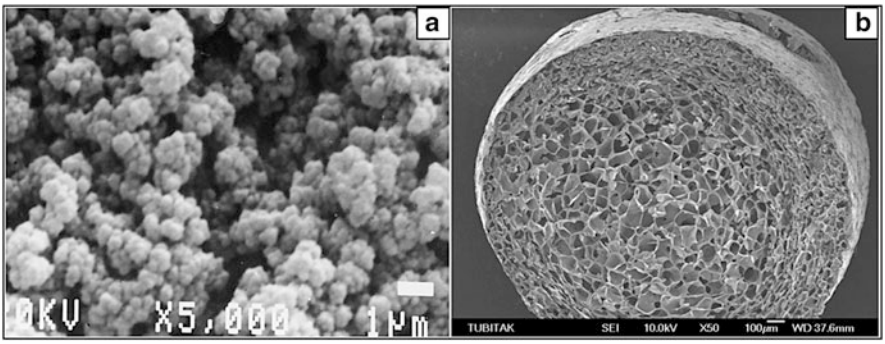

Fig. 1 SEM images of macroporous networks formed by (**a**) phase separation and (**b**) cryogelation techniques. **(a)** PNIPA network: C_o= 20 % (w/v); BAAm = 30 wt% (with respect to NIPA); T_{prep}=22.5 °C; diluent, water. (Reprinted from [14] with permission from Elsevier). **(b)** PAAm network: $T_{prep} = -18$ °C;C_o= 3 % (w/v); crosslinker ratio (molar ratio of BAAm to AAm) = 1:80. (From [23] with permission of Taylor & Francis Group, LLC). *Scale bars*: 1 µm (**b**), 100 µm (**b**)

structure was discovered at the end of the 1950s [11–13]. This technique involves the free-radical crosslinking copolymerization of the monomer–crosslinker mixture in the presence of an inert substance (the diluent or porogen), which is soluble in the monomer mixture. In order to obtain macroporous structures, a phase separation must occur during the course of the network formation process so that the two-phase structure formed is fixed by the formation of additional crosslinks [12]. After the polymerization, the diluent is removed from the network, leaving a porous structure within the highly crosslinked polymer network. This mechanism of porosity formation known as "reaction-induced phase separation" leads to the formation of macroporous gels consisting of agglomerates of polymer particles of various sizes that look like cauliflowers. Figure 1a shows a typical scanning electron microscopy (SEM) image of a poly(*N*-isopropylacrylamide) (PNIPA) gel network formed by the phase separation technique [14]. Although macroporous gels formed by phase separation exhibit a fast response rate to external stimuli [14], their aggregate-like morphology (consisting of rather weakly joined microgel particles) inevitably causes a significant reduction in their mechanical properties. Moreover, since a large amount of crosslinker has to be used to induce a phase separation during gelation, the network chains do not behave like flexible polymer chains sensitive to external stimuli.

Cryogelation is a simple strategy that allows the preparation of macroporous gels with high toughness and superfast responsivity. Although discovered over 30 years

the distance between the chains varies between zero and several nanometers depending on the external conditions. Further, removing the solvent from a homogeneous gel results in a polymer network that is nonporous. Thus, "porous gels" refers to materials having a dry state porosity, characterized by a lower density of the network due to the voids as compared to the density of the matrix polymer (see [11] for a detailed discussion).

ago [15–19], cryogels have attracted intense attention only in the last 10 years due to their extraordinary properties [20–22]. For instance, they do not display undesirable properties such as brittleness, which is commonly observed for macroporous gels formed by phase separation polymerization. Cryogels are very tough and can withstand high levels of deformation, such as elongation and torsion; they can also be squeezed almost completely without any crack propagation. The cryogelation technique is based on the natural principle that sea ice is less salty than sea water, i.e., the rejection of brine from freezing salt solutions. This principle is a consequence of the insolubility of the salts in ice compared to their excellent solubility in water. In cryogelation reactions, the reaction solution, generally containing the monomers and the initiator, is cooled below the freezing point of the system; since the monomers and the initiator will be enriched in the unfrozen microzones surrounded by solvent crystals, the polymerization reactions only proceed in these unfrozen regions containing a high concentration of monomer. The increased monomer concentration in the unfrozen reaction zones (i.e., cryo-concentration) is the main characteristic of the cryogelation reactions and is responsible for the extraordinary properties of cryogels. A macroporous structure in the final material appears due to the existence of solvent crystals acting as a template (or porogen) for the formation of the pores. The removal of template (e.g., ice) is achieved by simply holding the cryogel at temperatures above the solvent freezing point. This is another advantage of the cryogelation technique over the phase separation technique, where the latter requires extensive extraction of the gel to remove the porogen. In contrast to the cauliflower-like microstructure of macroporous gels formed by phase separation, cryogels exhibit a regular assembly of large pores of 10^0–10^1 μm in size separated by dense pore walls of several micrometers in thickness (Fig. 1b) [23].

This chapter discusses the conditions for formation of macroporous gels by the cryogelation technique. It also discusses how and why the properties of gels significantly alter upon transition from conventional gelation to the cryogelation regime. The formation and structure–property relationships of cryogels starting from monovinyl–divinyl monomers, as well as from linear polymer chains, are reviewed using examples from the recent literature. Some novel cryogels based on DNA, silk fibroin, poly(acrylic acid), and several types of rubbers with a wide range of tunable properties are also presented in details together with their applications.

2 Preparation and Characterization of Cryogels

Cryogels are mainly prepared by crosslinking polymerization of monomers or by crosslinking of linear polymers in frozen solutions. The most commonly used monomeric and polymeric precursors, the crosslinkers, the general preparation conditions, and characterization techniques are summarized in this section.

2.1 Monomeric and Polymeric Precursors, Crosslinkers

Several monovinyl–divinyl comonomer pairs have been used for the preparation of cryogels by free-radical crosslinking copolymerization. Mainly, water-soluble monomers have been used in the synthesis of cryogels, such as acrylamide (AAm) [16, 24–26], *N*,*N*-diethylacrylamide [27], *N*,*N*-dimethylacrylamide (DMA) [28–30], acrylic acid (AAc) [31], *N*-isopropylacrylamide (NIPA) [32–34], 2-hydroxyethyl methacrylate (HEMA) [35], and 2-acrylamido-2-methylpropane sulfonic acid sodium salt (AMPS) [36], in combination with *N*,*N*-methylene(bis) acrylamide (BAAm), poly(ethylene glycol diacrylate), or biodegradable crosslinkers [33, 35]. Nanosized clay particles (Laponite) can also be used as a multifunctional crosslinker in the preparation of cryogels exhibiting very high extensibility [34]. An ammonium persulfate (APS) and *N*,*N*,*N*′,*N*′-tetramethylethylenediamine (TEMED) redox initiator system is generally used to initiate the polymerization reactions. Since the decomposition of the radical initiators is temperature dependent, the reaction solutions should be cooled before addition of the initiator. Otherwise, gelation will start before freezing of the reaction system, resulting in the formation of conventional gels. Alternatively, polymerization inhibitors such as hydroquinone can be included in the reaction system to shift the onset of the reactions beyond freezing of the solution [23]. Cryogelation reactions can also be initiated by ultraviolet (UV) or electron-beam radiations so that the freezing time before the initiation step can be controlled [37–39]. Controlled radical polymerization techniques such as reversible addition-fragmentation chain transfer (RAFT) reactions have also been utilized for the preparation of cryogels both in aqueous and organic media [30, 40]. Inspired by the double-network (DN) technology developed by Gong and coworkers [6], DN cryogels with dual sensitivity have also been prepared by conducting the cryogelation reactions within the macropores of the single-network cryogels [41].

Cryogels can also be prepared starting from linear polymers in the presence of a chemical crosslinker in aqueous or organic solutions. Several natural and synthetic polymers have been used for the preparation of cryogels. The most popular crosslinker for proteins is glutaraldehyde, which is highly active towards the amine groups of a peptide chain in aqueous solutions. Proteins (e.g., gelatin, fibrinogen, collagen, and bovine serum albumin), polysaccharides (e.g., chitosan, hyaluronic acid), and synthetic polymers such as polyacrylamide (PAAm) and poly (vinyl alcohol) (PVA) can be crosslinked using glutaraldehyde in their frozen solutions [17, 42–44]. Cryogels were also prepared via crosslinking of amino end-functionalized star-shaped poly(ethylene glycol) with heparin in aqueous solutions [45]. However, it is not always necessary to use a crosslinker in the preparation of cryogels from polymeric precursors. For example, the hydrogen bonds formed between PVA chains in the unfrozen reaction phase lead to microcrystalline domains that act as crosslinkers in PVA cryogels [44, 46].

Di-epoxides such as ethylene glycol diglycidyl ether (EGDE) and 1,4-butanediol diglycidyl ether (BDDE) in the presence of TEMED catalyst have been used as

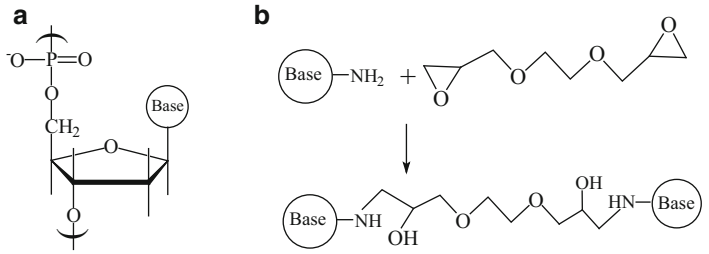

Scheme 1 (**a**) Nucleotide repeat unit of DNA and (**b**) the crosslinking reaction of the amino groups on the nucleotide bases with EGDE, leading to DNA cryogels

crosslinkers in the preparation of DNA and fibroin cryogels [47–50]. EGDE and BDDE contain epoxide groups on both ends that can react with nucleophiles such as amino groups, sulfhydryls, and hydroxyls. Because the amino groups on the nucleotide bases of DNA react with EGDE, heat-resistant interstrand crosslinks form during the cryogelation reactions, leading to the formation of DNA cryogels (Scheme 1) [48]. Silk fibroin cryogels can also be prepared using EGDE as a crosslinker. Here, EGDE crosslinks between the NH_2 groups of arginine and the lysine residues of fibroin molecules trigger the conformational transition of fibroin from the random coil to β-sheet structure and, hence, cryogel formation [49, 50]. Thus, fibroin cryogels contain both chemical crosslinks and β-sheet structures acting as physical crosslinks.

Rubber cryogels can be prepared using sulfur monochloride (S_2Cl_2) as a crosslinker [51–57]. Sulfur monochloride, a liquid at room temperature and soluble in organic solvents, is an effective crosslinker for the crosslinking processes of several types of rubbers, such as natural rubber, butyl rubber (PIB), *cis*-polybutadiene (CBR), and styrene-butadiene rubber (SBR) in organic media such as benzene, cyclohexane, and toluene [52, 53, 55]. The crosslinking reactions between the internal unsaturated groups of the rubbers via sulfur monochloride proceed in steps, as in the reaction between ethylene and sulfur monochloride (Scheme 2) [55]. Attack of sulfur dichloride on the internal vinyl group of the polymer leads to the formation of pendant sulfur chloride groups on the chains acting as potential crosslink points. Reaction of these groups with the internal vinyl groups on other chains is responsible for the formation of effective crosslinks.

Instead of linear polymers, micrometer-sized gel particles can also be used for the preparation of cryogels [58]. Such cryogels, with pore walls composed of close-packed particles, have been obtained by crosslinking of frozen aqueous suspensions of PNIPA gel particles or spherical and rod-shaped bacterial cells using glutaraldehyde as a crosslinker [58].

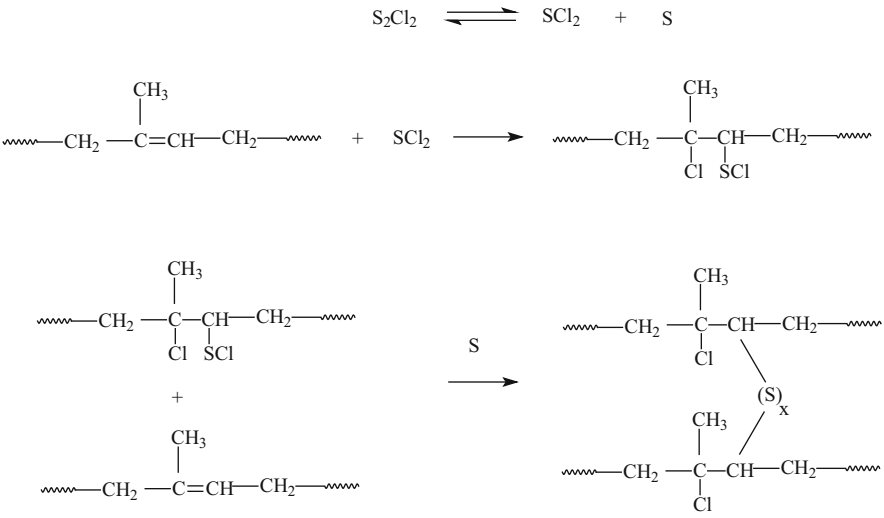

Scheme 2 Crosslinking reactions between the internal unsaturated groups of PIB via sulfur monochloride

2.2 Solvents and the Cryogelation Temperature

Water is cheap and benign to biological systems and, therefore, it is the most commonly used solvent in cryogelation reactions. Organic solvents such as dimethyl sulfoxide (DMSO) [32, 59], dioxane [24, 33, 40], formamide [24], nitrobenzene [60], benzene [52], and cyclohexane [53] with relatively high freezing points can also be used for the preparation of hydrophobic cryogels. Since the cryo-concentration of the reaction constituents in the unfrozen domains is a requirement for the formation of cryogels, the gelation temperature T_{prep} is the most important experimental parameter [61]. A so-called moderate temperature is commonly used for cryogelation reactions [62], which means a sufficiently low temperature, e.g., several degrees lower than the freezing point of the system. T_{prep} is usually set to 2–20 °C below the bulk freezing temperature of the solvent. In addition, the type of cooling of the reaction solution to T_{prep} also affects the cryogel properties. For example, liquid cooling provides much faster freezing of the reaction solution than air cooling, leading to the generation of smaller pores [52].

2.3 Monomer or Polymer Concentration

The initial concentration C_o of the monomeric or the polymeric precursors is another important parameter in cryogel preparation. Due to the effect of cryo-concentration, cryogels can be prepared at much lower concentrations compared

to the conventional gels [42]. For example, in the free-radical crosslinking copolymerization of AMPS and BAAm (17 mol % of the comonomer mixture) at $T_{prep} = -22$ °C, crosslinked polymer starts to form at $C_o = 0.1$ %, as compared to 5 % when conducted at $T_{prep} = 25$ °C [63]. In the preparation of PIB cryogels in benzene using S_2Cl_2 crosslinker (6 % v/w with respect to PIB), critical PIB concentration for gelation is 0.08 ± 0.02 % at −18 °C, compared to 4 % at $T_{prep} = 20$ °C [52]. Therefore, cryogels can be prepared over a wider concentration range compared to the conventional gels; however, since the cryogels formed at very low C_o are mechanically weak, the usual concentration range is between 2 and 20 % (w/v). Because increasing C_o or decreasing T_{prep} decreases the pore size of the cryogels and simultaneously increases their mechanical strength, these synthesis parameters can be used to tune the properties of cryogels.

2.4 Geometry of Cryogels

Cryogels can be prepared in various shapes such as blocks, sheets, discs, and beads [64]. Cryogels as continuous-bed columns (monoliths) for chromatographic separation of biomolecules have been prepared by filling the gelation solution in plastic syringes with a closed outlet at the bottom and then immersing the syringes in a cryostat at T_{prep} [29, 65–67]. To ensure the reproducibility of the freezing patterns, reaction mixtures of the same volume, and syringes of the same dimensions, should be used for every synthesis [68]. After completion of the cryogelation reaction, the cryogel blocks are thawed at room temperature and then thoroughly washed with a good solvent to remove unreacted species. Cryogels can also be prepared in the form of membranes by injecting the reaction solution between two glass plates separated by a spacer.

In contrast to blocks consisting of a single piece of macroporous material, cryogels in the form of beads are suitable for packing in columns with different scales. However, due to a number of preparation difficulties, there are only a few publications on the preparation of cryogel beads. For instance, if the cryogelation reactions are carried out under the conditions of the usual suspension polymerization technique, odd-shaped gel particles with a broad size distribution are obtained, due to collisions between the frozen droplets [69]. It was shown that cryogel particles can be prepared inside the wall of a hollow plastic carrier to make them resistant to intensive stirring [70]. Yun et al. utilized a microfluidic flow focusing technique to generate a suspension of aqueous gelation solution in a water-immiscible organic phase [71, 72]. After keeping the droplets at subzero temperatures, PAAm-based cryogel beads of 1 mm in diameter were produced. Alginate-agarose, PAAm, and DNA-based cryogel beads have been prepared recently by dropwise addition of the aqueous reaction solution into the paraffin oil as the continuous phase at temperatures between −15 and −20 °C [47, 64, 73]. The diameter of the cryogel beads could be adjusted by changing the tip diameter of

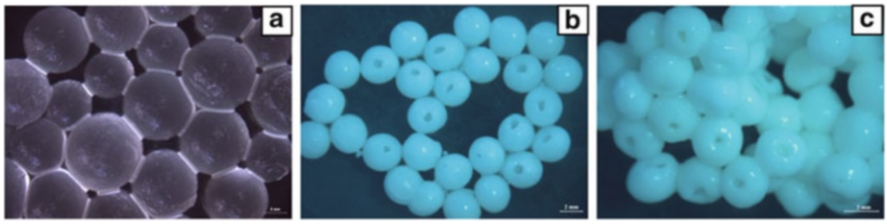

Fig. 2 Optical microscopy images of cryogel beads. (**a**) Ionic PAAc cryogel beads formed at −18 °C. (From [73] with permission from Elsevier). (**b**) Frozen PIB solution droplets in liquid nitrogen, and (**c**) crosslinked PIB beads just after preparation. S_2Cl_2 = 20 % (v/w); PIB concentration = 10 % (w/v). (From [69] with permission from Elsevier). *Scale bars*: 2 mm

the pipettes from which the aqueous phase was added into the oil phase. Figure 2a shows images of ionic PAAm cryogel beads prepared at −18 °C [73].

Preparation of hydrophobic cryogel beads have also been reported recently [69]. Cryogelation reactions were carried out within the droplets of frozen benzene solutions containing PIB and sulfur monochloride as a crosslinker. Spherical millimeter-sized PIB cryogel beads with a polydispersity of less than 10 % were obtained by use of two techniques. First, the reaction solution is dropped into liquid nitrogen to create small frozen organic droplets at −196 °C. Then, the frozen droplets are transferred into ethanol at −18 °C as the continuous phase, and the cryogelation reactions are carried out without stirring. Images in Fig. 2b show frozen solution droplets in liquid nitrogen, and Fig. 2c shows PIB beads just after preparation [69]. Freezing of PIB solution in liquid nitrogen results in the formation of uniform frozen solution droplets with an opening in their shells. The spherical shape and the morphology of the frozen droplets remain unchanged after the crosslinking reactions as well as after swelling of the crosslinked particles in toluene. The second technique involves dropwise addition of the organic solution into a continuous phase at −18 °C without stirring [69]. Here, the density of the continuous phase was so adjusted that the droplets slowly fall through the solution. An ethylene glycol–ethanol mixture (1:4 by volume) having a density close to that of the organic droplets was used as the continuous phase of the reaction. Similarly to the first technique, the resultant PIB beads have openings on their surfaces. Although the formation mechanism of a single large hole in the surface of the particle is still unclear, polymer/solvent phase separation during freezing and subsequent interfacial free energy minimization may be responsible for this process [74].

2.5 Morphological and Mechanical Characterization

Study of the macroporous structure of gels is a challenging task since there is no standard method for the pore-structure determination of such soft materials.

Although techniques such as optical microscopy, environmental scanning electron microscopy (ESEM), and confocal laser scanning microscopy (CLSM) can be used for the morphological characterization of cryogels in their swollen states, they do not lead to sufficient resolution to reveal the fine structure of cryogels. Due to the compressibility of gels under high pressure, other techniques such as mercury intrusion porosimetry and gas adsorption/desorption are not suitable for pore-structure characterization and can only be applied to dry materials. SEM is a suitable technique for characterizing the fine structure of cryogels; however, it also requires drying of the gel samples, which might result in structural changes. Nevertheless, it is assumed that freeze-drying and the sample preparation do not result in alteration of the pore structures due to the formation of dense pore walls during cryo-concentration. Therefore, SEM has been generally used to visualize the morphology and calculate the average pore size of cryogels. Moreover, the flow-through characteristics of cryogels in the form of blocks or beads can also be used to estimate their pore sizes and morphologies. More details about other characterization techniques used for cryogels can be found in recent reviews by Gun'ko and Savina [75, 76].

The total volume of open pores V_p of the cryogels can easily be estimated through uptake of a poor solvent, such as acetone for PAAm or methanol for PIB cryogels. Since a poor solvent for polymer can only enter into the pores of polymer networks, V_p (milliliters of pores in 1 g of dry polymer network) can be calculated as:

$$V_p = \frac{(m_{NS} - m_{dry})}{m_{dry}\, d_1} \tag{1}$$

where m_{NS} and m_{dry} are the weight of the cryogel in the poor solvent and its dry weight, respectively, and d_1 is the solvent density. The total porosity P of dried cryogels (milliliters of pores in 1 mL of dry polymer network) can be estimated from their densities as:

$$P = 1 - \frac{d_0}{d_2} \tag{2}$$

where d_o is the apparent density(i.e., density of the porous network) and d_2 is the (nonporous) polymer density. The relative values of the equilibrium volume (q_v) and the equilibrium weight swelling capacities (q_w) of the cryogels also provide information about their internal structure in the swollen state. These swelling ratios are calculated as:

$$q_v = (D/D_{dry})^3 \tag{3a}$$

$$q_w = (m/m_{dry}) \tag{3b}$$

where D and D_{dry} are the gel diameters in equilibrium swollen and dry states, respectively, and m is the weight of equilibrium swollen gel. During the cryogel swelling process, the pores inside the cryogel network are rapidly filled with the solvent; at the same time, the network region making up the pore walls of the cryogel takes up solvent from the environment by diffusion process. Therefore, the swelling of cryogels is governed by two separate processes: (1) solvation (swelling) of the pore walls and (2) filling of the pores by the solvent.

The equilibrium weight swelling ratio q_w includes the amount of solvent taken up by both of these processes. By contrast, if we assume isotropic swelling (i.e., the volume of the pores remains constant upon swelling), the volume swelling ratio q_v of cryogels is caused by solvation of the pore walls, i.e., by the first process. Thus, q_v only includes the amount of solvent taken up by the gel portion of the cryogel network. Accordingly, the higher the difference between q_w and q_v, the higher is the volume of the pores in swollen cryogels. The swollen state porosity P_s of the cryogels can be estimated from their volume and the weight swelling ratios using the equation [11]:

$$P_s = 1 - \frac{q_v}{1 + (q_w - 1)\, d_2/d_1} \tag{4}$$

Several techniques are available for the mechanical characterization of cryogels in swollen and dried states. Uniaxial compression tests are conducted on cylindrical cryogel samples to determine the Young's modulus E or shear modulus G from the slope of stress–strain curves at low compressions, while the stress at 3 or 5 % compression is reported as the compressive stress σ_{comp}. For uniaxial compression of a cylindrical gel sample, the statistical theories of rubber elasticity yield for Gaussian chains an equation of the form [77, 78]:

$$\sigma = G\left(\lambda - \lambda^{-2}\right) \tag{5a}$$

where σ is the nominal stress and λ is the corresponding deformation ratio (deformed length/initial length). In contrast to a cylindrical cryogel sample, the interpretation of the compression test data of a spherical cryogel particle is complicated. This is due to significant variation in the contact area between the wall and the originally spherical gel during deformation. For a sphere with a constant volume during deformation, the Hertz equation can be used to estimate the modulus of cryogel beads [79–84]:

$$F = \frac{4}{3} G D_1^{0.5} \Delta D^{1.5} \tag{5b}$$

Here, F is the force and ΔD is the deformation, $\Delta D = D_1 - D_2$,where D_1 and D_2 are the initial undeformed and deformed diameters of the sample, respectively. According to (5b), a linear relation is expected if $(3/4)FD_1^{-0.5}$ is plotted against $\Delta D^{1.5}$ with a slope equal to the modulus G of the beads. Indeed, linear plots were

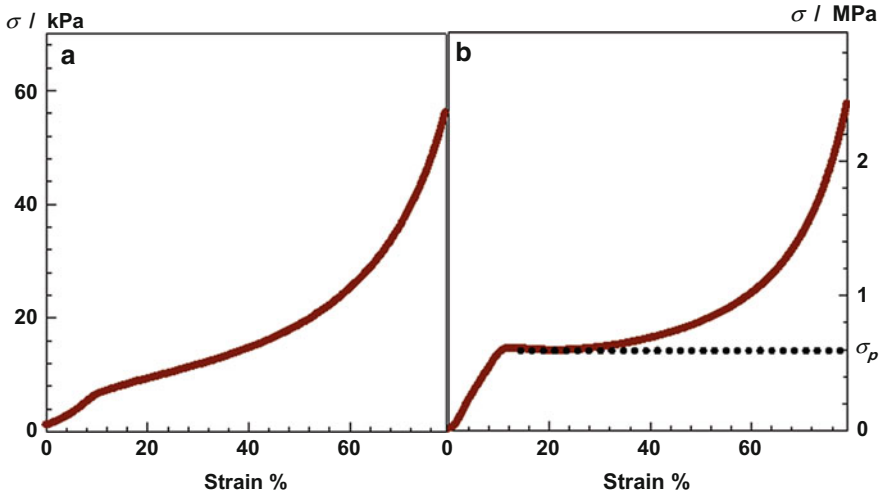

Fig. 3 Stress–strain curves of a fibroin cryogel in (**a**) swollen and (**b**) dry states are shown as the dependence of the nominal stress σ on the degree of compression; $T_{prep} = -18$ °C; $C_{SF} = 4.2$ %; EGDE = 20 mmol/g epoxide; TEMED = 0.07 %

obtained for both hydrophilic and hydrophobic cryogel beads [47, 69, 73]. It was shown that the modulus (i.e., the effective crosslink density of the cryogel beads) decreases with decreasing bead diameter [73]. This size-dependent crosslink density of the beads is attributed to the fact that the gelation reactions at the surface layer of the droplets slow down due to the contact of this region with the continuous phase. This will reduce the crosslink density of the surface layer of the resulting gel beads. Since decreasing the size of the droplets increases the surface-to-volume ratio of the final beads, the smaller the bead diameter, the smaller its average crosslink density.

The large strain properties of some spongy cryogels can also be investigated by uniaxial compression tests up to complete compression. Typical stress–strain curves of cryogels in swollen and dry states are shown in Fig. 3a, b as the dependence of nominal stress σ on percentage compression [50]. During compression of the swollen cryogel, the curve is quite linear up to a critical strain, indicating that the pores filled with solvent remain mechanically stable. As the cryogel is further squeezed under the piston, the pores gradually release solvent due to buckling of the pore walls so that it can easily be compressed. Similarly, the stress–strain curve of the dried cryogel is first linear, indicating that the macroporous structure remains mechanically stable in this range of strain. This linear elastic regime is followed by a near-plateau regime, indicating that the network easily deforms due to the collapse of its pores under the pressure. The critical stress corresponding to the plateau regime, denoted by σ_p in Fig. 3b, is a measure of the mechanical stability of the porous structure of cryogels. Finally, the steep increase of the curve in the third regime corresponds to the compression of the

nearly nonporous polymer network. Although freeze-dried hydrogels are also porous, no distinct plateau is observed in stress–strain curves [50], which is attributed to the weak network structure due to the absence of cryo-concentration.

Squeezability of the cryogels and their reusability, as well as the continuous extraction capacity for the removal of pollutants, are determined by subjecting the cryogel samples to successive sorption–squeezing cycles under identical conditions. In a typical procedure [54], the cryogel sample is first immersed in the test solution for 1 min and then it is left to drip for 30 s. The cryogel is weighed and put into a Büchner funnel and squeezed for 30 s under 50 mm vacuum. Then, it is weighed again to calculate the amount of solution taken up by one gram of cryogel. This sorption–squeezing cycle is repeated many times to obtain the recycling efficiency and continuous extraction capacity of the cryogels.

3 Transition from Gelation to Cryogelation: Gels Versus Cryogels

Since cryo-concentration is a characteristic phenomenon of cryogelation, it is necessary first to discuss how increased monomer concentration at gelation affects the properties of conventional gels. Several studies show that the gel structure and, thus, the gel properties strongly depend on the initial monomer concentration [11, 13, 85–89]. No continuous network is formed below a critical concentration of monomer. Increasing the amount of monomer at polymerization causes the polymer chains to entangle so that the network formed in a semidilute solution can swell poorly, even when exposed to a good solvent. This increase in the monomer concentration also decreases the probability of cyclization reactions, so that a large fraction of the crosslinker is consumed in effective crosslinks [85]. In accord with the experiments, the statistical model proposed by Bromberg et al. predicts that the effective crosslink density of gels scales with the second power of the monomer concentration [89, 90]. As a consequence, the network structure formed becomes increasingly tight as the monomer concentration increases.

Let us now consider what will happen to the monomer concentration when the polymerization temperature is decreased below the freezing point of the reaction system. During freezing, the monomers and the initiator are expelled from the forming solvent crystals and become entrapped within channels between the crystals. As a consequence, the polymerization reactions can only take place in spatially restricted reaction fields, which are the unfrozen microchannels of the apparently frozen system. The reason why solvent does not freeze below the bulk freezing temperature is attributed to the freezing point depression of the solvent due to the solutes, e.g., monomers and polymers [91–93]. For instance, about 6 % of the water in swollen PAAm hydrogels remains unfrozen, even at −24 °C [26]. Kirsebom used ^{1}H NMR to estimate the monomer concentration in the unfrozen microchannels [28]. The reaction system studied was the crosslinking copolymerization of DMA

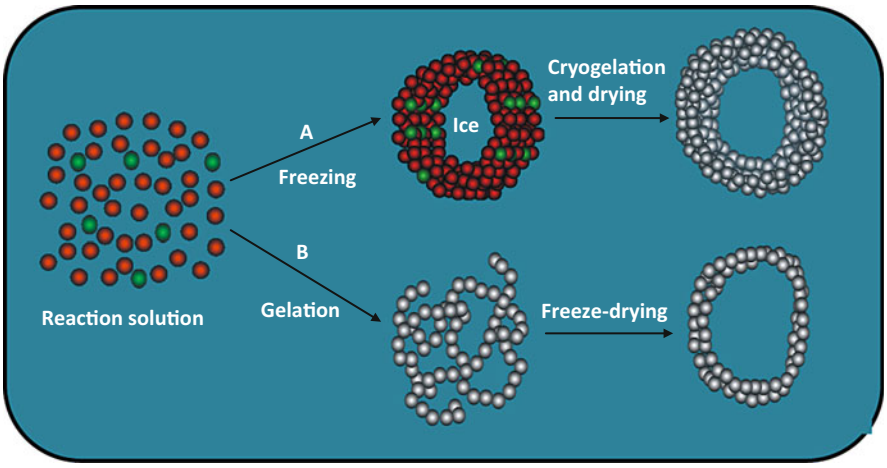

Fig. 4 Formation process of a pore by cryogelation (**a**) and by freeze-drying (**b**). *Red*, *green*, and *gray* circles represent monovinyl monomers, divinyl monomers, and polymer repeat units, respectively

and poly(ethylene glycol) diacrylate in aqueous solutions. It was found that the local concentration of the monomers in the unfrozen zones was 32.6 and 45.5 wt% at $T_{prep} = -10$ and -20 °C, respectively, as compared to the initial (nominal) monomer concentration of 6 wt% [28]. Thus, the actual concentration of the monomer in the microchannels is about sixfold larger than its nominal concentration. As a consequence, the critical monomer concentration for the onset of gelation is much lower in cryogelation compared to the conventional gelation systems. This cryo-concentration effect is also responsible for the fact that a high polymer content of the gel phase produces thick and dense pore walls in the resulting cryogels.

The transition from conventional gelation to the cryogelation regime requires that the cryo-concentration of reaction constituents occurs before onset of the gelation reactions. For instance, freeze-drying of an already formed gel does not lead to materials with cryogel properties due to the formation of ice crystals in a gel rather than in a solution. This is illustrated schematically in Fig. 4, which compares the formation process of a pore by cryogelation and by freeze-drying. The pore wall produced by cryogelation is a dense polymeric gel because of the cryo-concentrated solution of the monomers around the ice crystals. In contrast, the pore wall formed after freeze-drying of a conventional gel is a loosely crosslinked gel due to the absence of cryo-concentration. As a consequence, the porous structures produced during cryogelation are mechanically stable, even under large strain conditions. Typical images of swollen and freeze-dried hydrogel and cryogel samples formed from aqueous silk fibroin solutions are shown in Fig. 5 [50]. The gels were prepared under identical conditions except that the gel preparation temperature, T_{prep}, was $-$ 18°C for the cryogel and 50 °C for the hydrogel [50]. After freeze-drying, the

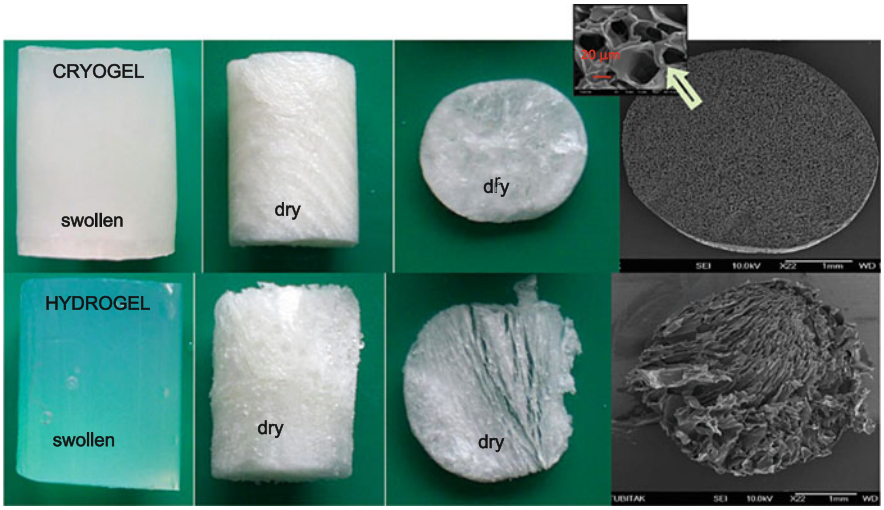

Fig. 5 Images of the cryogel (*top row*) and hydrogel samples (*bottom row*) formed at −18 and 50 °C, respectively, in swollen and dry states. C_{SF} = 4.2 wt% EGDE = 20 mmol/g; TEMED = 0.10 %. *Scale bars*: 1 mm (SEM images on *far right*), 20 μm (*inset*). (From [50] with permission from the American Chemical Society)

scaffold derived from the cryogel retains its original shape, whereas a lateral distortion in the cylindrical shape of the hydrogel scaffold is observed. SEM images of these samples (Fig. 5) also show that the cylindrical shape of the hydrogel scaffold is partially destroyed due to the weak network structure. In contrast, cryogel scaffold is mechanically stable and consists of regular, interconnected pores of diameters from 5 to 10 μm that are separated by thick pore walls.

How does the local concentration of the monomer in the unfrozen reaction zones vary depending on the cryogelation conditions? What is the volume fraction of frozen solvent in the reaction system? A simple thermodynamic model was recently developed to answer these questions [36]. The model considers a polymeric gel in equilibrium with a solvent at a given temperature. As the temperature is decreased below the freezing temperature of the solvent, solvent freezes out of the gel phase so that a two-phase system forms that consists of pure solvent crystals and an unfrozen gel. The equilibrium condition between these two phases at a given temperature T_{prep} is such that the chemical potentials of solvent crystals (μ_1^{cry}) and of liquid solvent in the gel (μ_1^{gel}) must be equal. μ_1^{gel}in the gel phase is $\mu_1^{gel} = \mu_1^{o} + RT_{prep}\ ln\ a_1$, where μ_1^{o} is the chemical potential of pure liquid solvent and a_1 is the activity of solvent in the gel. Equating μ_1^{cry} and μ_1^{gel} at T_{prep} and, since $\mu_1^{o} - \mu_1^{cry}$ equals the molar Gibbs free energy change for melting of solvent crystals, one obtains:

$$\ln a_1 = \frac{\Delta H_m}{R}\left(\frac{1}{T_f^0} - \frac{1}{T_{\text{prep}}}\right) \quad (6)$$

where ΔH_{m} and $T_{\text{f}}{}^0$ are the molar enthalpy of fusion and the normal freezing point of pure solvent, respectively, and R is the gas constant.[2] The Flory–Rehner theory including the ideal Donnan equilibria gives the following relation between the activity of a swelling agent (solvent) in the gel and the gel parameters [77]:

$$\ln a_1 = \ln(1-\nu_2) + \nu_2 + \chi\nu_2^2 + \nu_{\text{e}}V_1\left[\nu_2{}^{1/3}\left(\nu_2^0\right)^{2/3} - 0.5\nu_2\right] - f\nu_2 \quad (7)$$

where ν_2 and ν_2^0 are the volume fractions of crosslinked polymer in the equilibrium swollen gel and after gel preparation, respectively, χ is the polymer–solvent interaction parameter, ν_{e} is the effective crosslink density of the network, V_1 is the molar volume of solvent, and f is the effective charge density, i.e., the fraction of charged units in the network chains that are effective in gel swelling. Since $\nu_2 = \nu_2^0$ after cryogel preparation, substituting (7) into (6) yields [36]:

$$\frac{1}{T_{\text{prep}}} = \frac{1}{T_{\text{f}}^0} - \frac{R}{\Delta H_{\text{m}}}\left[\ln\left(1-\nu_2^0\right) + \nu_2^0 + \chi\left(\nu_2^0\right)^2 + 0.5\nu_e V_1 \nu_2^0 - f\nu_2^0\right] \quad (8)$$

Using (8), one may estimate the polymer concentration ν_2^0 in the unfrozen gel phase at a given temperature T_{prep} ($T_{\text{prep}} < T_{\text{f}}{}^0$). To apply (8) to the cryogelation systems, we assume that the monomers completely accumulate in the unfrozen reaction phase before the onset of gelation. We also assume that, after cryogelation, the conversion of monomer to crosslinked polymer is complete. Thus, the monomer concentration C in the unfrozen zones (in % w/v) can be estimated from ν_2^0 as:

$$C = \left(\nu_2^0 d_2\right)10^2 \quad (9)$$

The volume fraction of frozen solvent in the reaction system, P, can also be estimated as:

$$P = 1 - \frac{C_{\text{o}}}{C} \quad (10)$$

where C_{o} is the nominal monomer concentration. Since the frozen solvent acts as a template in the cryogels, P also corresponds to their porosities (volume of pores/

[2] Assuming ideally dilute solutions, (6) leads to the well-known equation $T_{\text{prep}} - T_f^0 = -K_f m_2$, where K_{f} is the freezing-point-depression constant, and m_2 is the solute molality. However, this equation cannot be used for the cryogelation system due to the high concentration of solutes in the unfrozen domains.

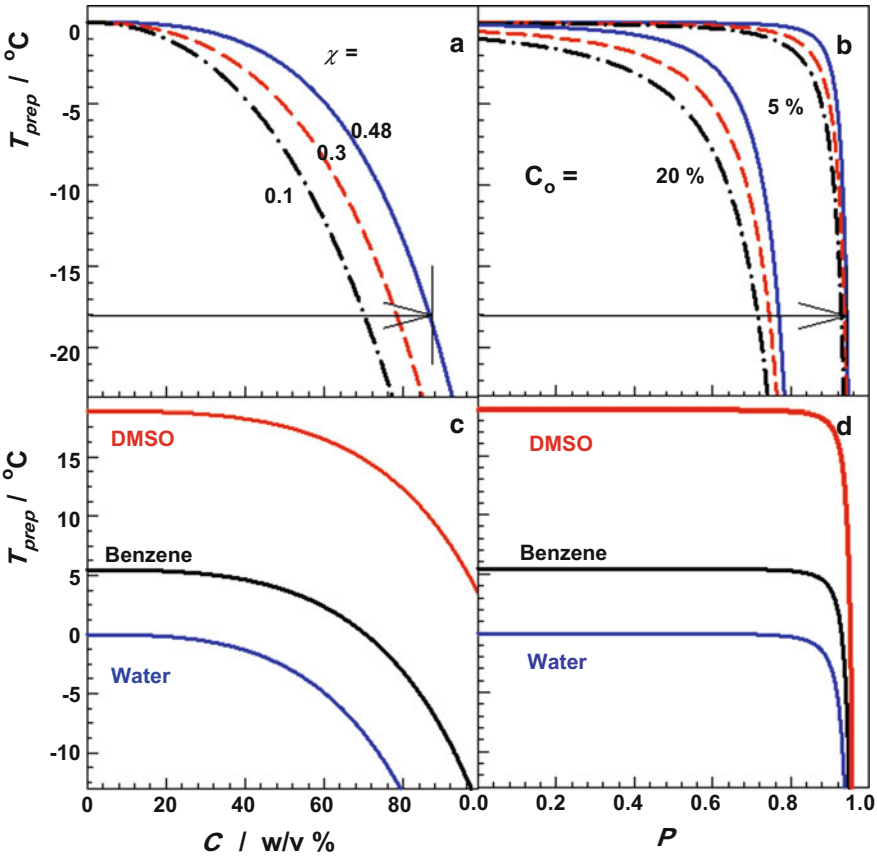

Fig. 6 (**a**, **c**) Monomer concentration C in the unfrozen gel phase and (**b**, **d**) volume fraction of frozen solvent in the cryogels P shown as a function of the temperature T_{prep}. (**a**, **b**) The solvent was water. Calculations are for various χ parameters indicated. P was calculated for $C_o = 5$ and 20 %. (**c**, **d**) $\chi = 0.48$; $C_o = 5$ %. Calculations are for the various solvents indicated: $\nu_e = 20$ mol/m^3; ΔH_m (V_1, T_f^o) = 6.01 kJ/mol (18 mL/mol, 0 °C), 9.9 kJ/mol (89 mL/mol, 5.4 °C), and 14.4 kJ/mol (71.03 mL/mol, 19 °C) for water, benzene, and DMSO, respectively. The *arrows* in **b** and **c** illustrate the increase in monomer concentration in the unfrozen phase and the volume of frozen solvent at $T_{prep} = -18$ °C

cryogel volume). According to (8), the nominal monomer concentration C_o does not influence the monomer concentration C in the unfrozen phase; however, decreasing C_o, i.e., increasing water content, increases the porosity of cryogels at a given temperature T_{prep}.

Calculations using (8) show that the temperature T_{prep} significantly affects the monomer concentration in the unfrozen phase. Figure 6a, b shows how the monomer concentration C in the unfrozen domains and the volume fraction of frozen solvent in the resulting cryogel P vary with the temperature T_{prep}. Calculations were for water as the solvent and for various polymer–solvent interaction parameters χ

indicated in the figure (χ is assumed to be independent of temperature). Let us first consider the solid curve in Fig. 6a, which was calculated for $\chi = 0.48$, corresponding to polyacrylamide–water system [94]. At $T_{prep} = -18$ °C, as indicated by the arrow, C is predicted to be 86 %. This means that, as the solvent crystallizes at −18 °C, the monomer concentration in the unfrozen phase rises continuously until attaining its equilibrium value of 86 %. For an initial monomer concentration (C_o) of 5 %, P becomes 0.94 (Fig. 6b), indicating that 94 % of the reaction system consists of solvent crystals acting as template for pore formation. Increasing the initial monomer concentration from 5 to 20 % decreases the volume fraction of frozen solvent, i.e., porosity from 94 to 77 %. Figure 6a, b also shows that the lower the T_{prep}, the higher the monomer concentration in the reaction zones and the larger the porosity.

Moreover, decreasing the χ parameter at a given T_{prep} (i.e., increasing the solvating power of the solvent) also decreases the monomer concentration in the unfrozen zones and, thus, the total volume of the pores in the final cryogels. This is attributed to the increasing amount of uncrystallizable solvent bound to polymer chains as the quality of the diluent is increased. Figure 6c, d presents the results of calculations for three different solvents. As the temperature drops below the freezing temperature of the pure solvent, which is 0, 5.4, and 19 °C for water, benzene, and DMSO, respectively, the monomer concentration in the unfrozen zones rapidly increases. Cryogels with 95 % porosities could be obtained at $T_{prep} = -3$, +3, and +17 °C using water, benzene, and DMSO as the polymerization solvent, respectively. Thus, the cryogelation temperature can be adjusted by selecting a suitable solvent. As will be seen in the following sections, the prediction of simulation results is in qualitative agreement with the experimental findings.

The theoretical results in Fig. 6 also show that cryo-concentration and the resulting transition from gelation to the cryogelation regime occurs at temperatures close to the freezing point of the pure solvent. As a result, a drastic change in the gel properties has to be expected at these temperatures. For instance, increased monomer concentration due to cryo-concentration would lead to a significant increase in the elastic modulus and a decrease in the swelling capacity of the gels.

This was indeed observed experimentally, but at lower temperatures. The results of such measurements are shown in Fig. 7a–c for PAAm hydrogels, where the elastic modulus G, the equilibrium weight q_w, volume swelling ratio q_v of the gels, and their dry and swollen state porosities, P and P_s, respectively, are plotted against T_{prep} [26]. The gels were prepared by free-radical crosslinking copolymerization of AAm with BAAm in aqueous solution at various T_{prep} between −25 °C and +25 °C [26]. The dotted rectangular area in Fig. 7a–c indicates the transition between homogeneous gelation and cryogelation regimes occurring between −6 and −10 °C. Depending on T_{prep}, two types of gels can be obtained:

1. At $T_{prep} \geq -6$ °C: The gels exhibit a relatively low modulus of elasticity around 1.5 kPa. Both the weight q_w and the volume swelling ratios q_v of gels are equal to ~20, and they are independent of T_{prep}.
2. At $T_{prep} \leq -10$ °C: Decreasing T_{prep} below –6 °C results in a fourfold increase in the elastic modulus of gels. Moreover, the weight swelling ratio q_w remains

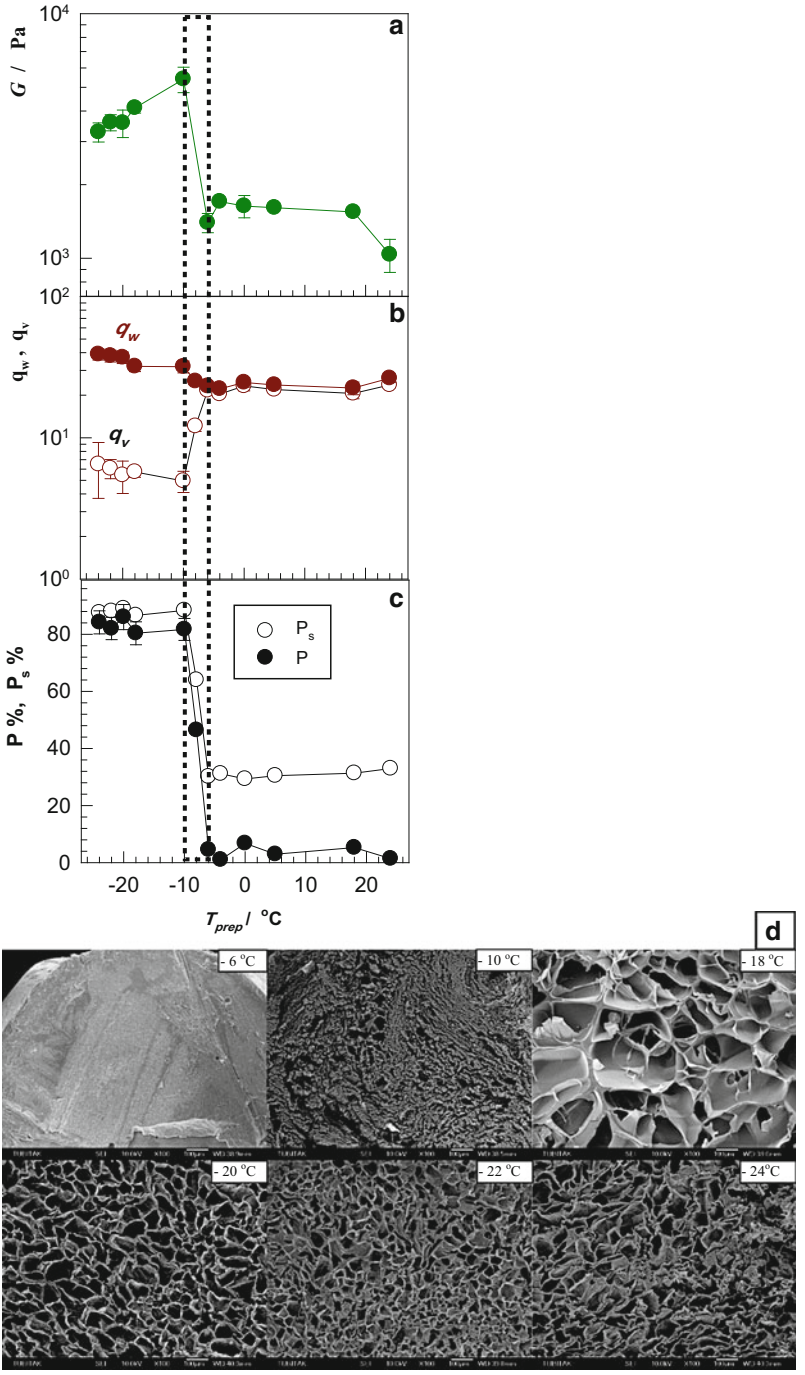

Fig. 7 (**a**) The elastic modulus G, (**b**) the equilibrium weight q_w and volume swelling ratios q_v, and (**c**) the swollen state porosity P_s and the dry state porosity P of PAAm gels shown as functions of the cryogelation temperature T_{prep}. (**d**) SEM images of PAAm networks formed at the various

almost unchanged as T_{prep} is decreased below −6 °C while the volume swelling ratio q_v rapidly decreases. At $T_{prep} \leq -10$ °C, the gels swell about sixfold more by weight than by volume. According to (4), these results suggest the appearance of pores in the gel matrices prepared at $T_{prep} \leq -10$ °C.

Indeed, the gels formed at $T_{prep} \geq -6$ °C were transparent, whereas those formed below –6 °C were opaque and exhibited 85 % porosities [26]. The total volume of pores, V_p, of the hydrogels estimated from the uptake of a poor solvent (cyclohexane) was in the range of 3–6 mL/g for the gels prepared below −6 °C, whereas those formed at higher temperatures exhibited negligible pore volumes. The SEM images in Fig. 7d illustrate the microstructure of the networks formed at various T_{prep}. All the polymer samples formed below –6 °C have a porous structure with pore diameters of 10–70 μm, whereas those formed at or above –6 °C exhibit a continuous morphology. At –10 °C, the pore walls seem to be too weak, so that they are more or less fused together to form large aggregates. Thus, the drastic change in the network microstructure induced by lowering T_{prep} from −6 to –10 °C is reflected by the swelling and elasticity tests, with decreasing volume swelling ratio and increasing modulus of elasticity of gels.

Similar results were also reported for polyelectrolyte hydrogels prepared from AMPS or sodium acrylate (SA) monomers with BAAm crosslinker in aqueous solutions [36, 95]. At $T_{prep} \geq -8$ °C, ionic hydrogels derived from AMPS exhibit relatively high volume swelling ratios V_{eq} of the order of 10^1 and low moduli of elasticity G in the range of 10^2–10^3 Pa [36]. Decrease of T_{prep} below –8 °C results in a tenfold decrease in the swelling ratio and about tenfold increase in the elastic modulus of gels. Moreover, the gels formed at or above –8 °C were transparent, whereas those formed at lower temperatures were opaque, indicating that these gels have separate domains in a spatial scale of submicrometer to micrometer [36]. Thus, the transition from homogeneous gelation to the cryogelation regime and the drastic change in the properties of poly(AMPS) (PAMPS) hydrogels appear if T_{prep} is decreased below –8 °C. In poly(sodium acrylate) (PSA) cryogels, this transition was observed atT_{prep} between −6 and −9 °C [95].

Experiments were also carried out to investigate the transition to the cryogelation regime in organic media. For this purpose, solution crosslinking of PIB was carried out using sulfur monochloride as a crosslinker in cyclohexane (freezing point = 6.5 °C) at various temperatures T_{prep} between −22 and 20 °C [53]. The organogels formed at $T_{prep} > -2$ °C were nonporous, whereas those formed at lower temperature were porous and exhibited typical cryogel morphologies with a total volume of pores of about 2.5 mL/g [53]. Thus, the transition to the cryogelation regime occurs at around −1 °C, i.e., about 8 °C below the freezing point of cyclohexane.

Figure 8 compares the response rate of PIB gels formed at temperatures both below and above the transition temperature [53]. Here, the normalized gel mass m_{rel}

Fig. 7 (continued) T_{prep} indicated. $C_o = 5$ % (w/v), X =1/80. *Scale bars*: 100 μm. Magnification 100×. (Reprinted from [26] with permission from Elsevier)

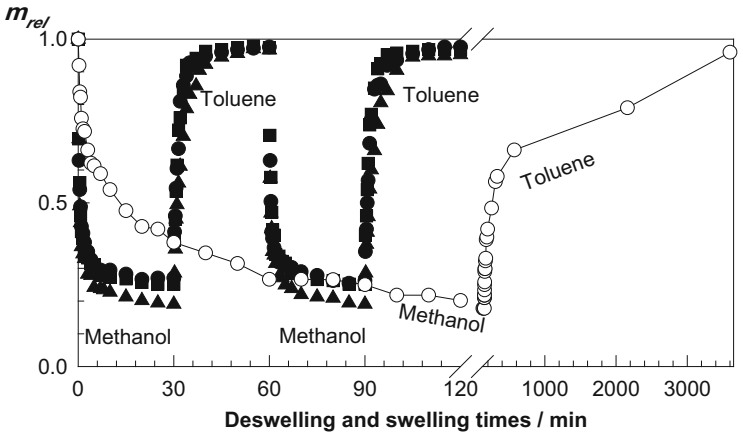

Fig. 8 The normalized mass m_{rel} of PIB gels shown as a function of the time of deswelling in methanol and re-swelling in toluene. S_2Cl_2= 5.7 %; reaction time = 3 days. $T_{prep} = -2$ (*filled triangle*), −10 (*filled circle*), −18 (*filled square*), and 17 °C (*open circle*). (Reprinted from [53] with permission from Elsevier)

(mass of gel at time *t*/equilibrium swollen mass in toluene) is plotted against the time *t* of deswelling in methanol and re-swelling in toluene. Both the swelling and deswelling rates of the gel prepared at subzero temperatures are much faster than those prepared at 17 °C; the low-temperature gels undergo two successive deswelling–swelling cycles before the room-temperature gel assumes its equilibrium collapsed conformation in methanol. They also exhibit reversible swelling–deswelling cycles, i.e., the gels return to their original shape and original mass after a short reswelling period. The collapsed gel formed at 17 °C reswells again within 3 days, compared to 10 min for gels formed at subzero temperatures. Similar results were reported for several cryogels formed below the transition temperature [26, 36, 63, 96]. For example, strong polyelectrolyte PAMPS cryogels prepared below –8 °C exhibit completely reversible swelling and deswelling cycles in water and acetone, respectively [36]. Those formed at higher temperatures were too soft in their swollen states in water; during the first deswelling process in acetone, they were broken into several pieces so that a cycle could not be completed. We have to note that cryogels starting from their dry states swell much faster than their collapsed states in equilibrium with a poor solvent. For example, PAAm cryogel, when collapsed in acetone, swells within 1 min to attain its equilibrium swollen state in water, whereas swelling takes only 4 s starting from its dry state [26]. The relatively slower rate of swelling of collapsed cryogels compared to dry gels is related to the nonsolvent molecules on the surface of the collapsed gel samples, which decrease the solvating power of the liquid around the gel sample and slow down the swelling process.

The mechanical properties of gels also change significantly below the transition temperature due to the cryo-concentration phenomenon. This is illustrated in

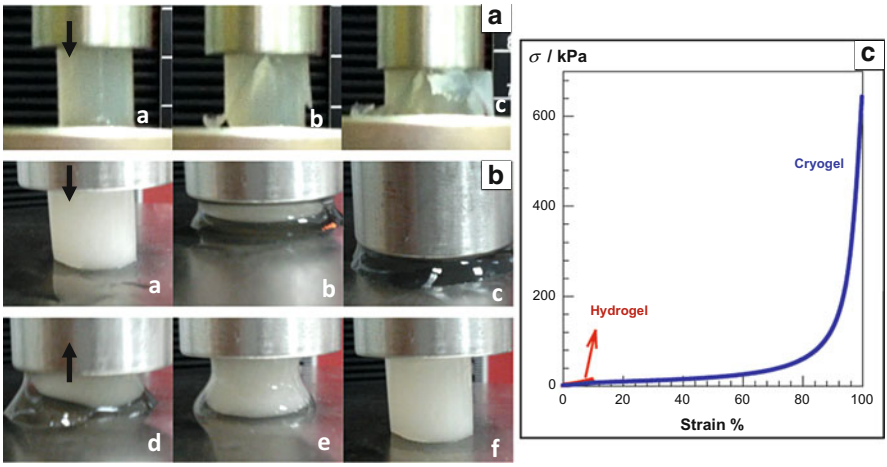

Fig. 9 Photographs of (**a**) fibroin hydrogels and (**b**) cryogels formed at T_{prep} =50 and −18 °C, respectively, during the compression tests. $C_{SF} = 4.2$ %; EGDE = 20 mmol/g; TEMED = 0.10 %. A*rrows* indicate the direction of piston movement. **(c)** Stress–strain curves of these gel samples are shown as the dependence of the nominal stress σ on the degree of compression. (From [50] with permission from the American Chemical Society)

Fig. 9a, b, which shows images of fibroin gels formed above and below the transition temperature, respectively [50]. The fibroin hydrogel formed at 50 °C ruptures under low deformation, indicating that the mechanical stress applied is localized without effective dissipation. However, fibroin cryogel formed at −18 °C remains mechanically stable up to almost complete compression. An important point is that, as the cryogel is squeezed under the piston or via manual hand compression, the gel releases all its water from within the pores so that it can be compressed up to 99.8 % compression ratio. Although no energy dissipation mechanism was introduced in the cryogels, release of water from the pores under stress seems to prevent crack formation at large deformation ratios. After release of the load, the gel sample immediately recovers its original shape by absorbing the released water. Figure 9c shows the stress–strain curves of these gel samples under compression. The hydrogel ruptures at about 10 % compression and at a compressive nominal stress of 15 kPa, whereas the cryogel sustains 99.8 % compression at 640 kPa stress. Successive compression tests conducted on the same gel sample between 0 and 99.8 % strain show reversibility of the stress–strain curves of the cryogels and reveal that no cracking occurs during the experiments [50]. The improved mechanical properties of cryogels originate from the high polymer content of the unfrozen liquid channels of the reaction system. Thus, after cryogelation, the gel channels with high polymer content are perfect materials for building the pore walls.

The experimental results thus indicate that the formation of cryogels requires a temperature T_{prep} of at least 8 °C below the bulk freezing temperature of solvent. In contrast, however, the theoretical results given in Fig. 6 predict that this transition

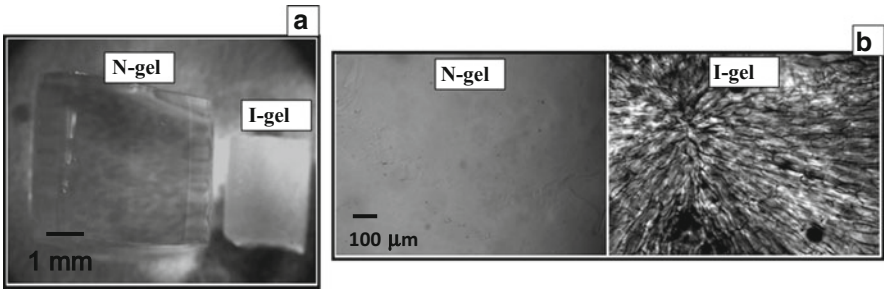

Fig. 10 (**a**, **b**) Different magnification images of swollen PAMPS gel samples taken using the optical microscope. The gels were prepared without (N-gel) and with precooling of the reaction solution (I-gel). $T_{prep} = -2\ ^{\circ}C$, $X = 1/6$. The initial diameters of the gel samples were 4.3 mm. In their swollen states, the diameters became 9.80 mm (N-gel) and 4.65 mm (I-gel). *Scale bars*: 1 mm (**a**) and 100 μm (**b**). (From [23] with permission from Taylor & Francis Group, LLC)

should occur at temperatures close to the solvent freezing temperature. This discrepancy may partially be attributed to the nonequilibrium effects during freezing [91]. The concentrated unfrozen polymer solutions at low temperatures have high viscosities that may slow down the equilibration of solvent and the growth of solvent crystals to an extent that stops freezing. Moreover, the initial non-isothermal reaction period may also be responsible for the observed deviation from theory. We have to mention that T_{prep} is the temperature of the thermostated bath in which the gelation reactions are carried out. Since the polymerization initiator (or crosslinker) should be added into the monomer (or polymer) solution before freezing of the reaction system, the polymerization and crosslinking reactions proceed non-isothermally from the moment of initiator addition to the moment when the temperature of the reaction system reaches T_{prep}. Therefore, the time needed for bulk freezing of the reaction system strongly depends on T_{prep}. For example, aqueous reaction mixtures containing AMPS and BAAm at $T_{prep} = -22\ ^{\circ}C$ became frozen within 4–5 min, whereas those at $-5\ ^{\circ}C$ required more than 1 h for freezing [36]. Compared to these freezing times, the gelation time recorded using the falling-ball technique was 5 min at $0\ ^{\circ}C$ [36]. Thus, gelation and gel growth reactions at $T_{prep} = -5\ ^{\circ}C$ mainly proceed before the onset of bulk freezing of the system, whereas the reactions at $-22\ ^{\circ}C$ occur in the unfrozen microzones. Therefore, variation in the cooling rate depending on T_{prep} may also be responsible for the appearance of porous structures at temperatures much below the bulk freezing point of the reaction system. This also suggests that isothermal gelation could provide formation of cryogels at a temperature close to the freezing point of the solvent.

To check this point, experiments were designed to control the freezing of the reaction solutions [23]. Figure 10a shows the images of two equilibrium swollen PAMPS gel samples prepared at $T_{prep} = -2\ ^{\circ}C$. Both the gel samples were prepared under identical conditions except for the initial temperature of the gelation system. In the case of the isothermal gel (I-gel), after addition of the initiator into

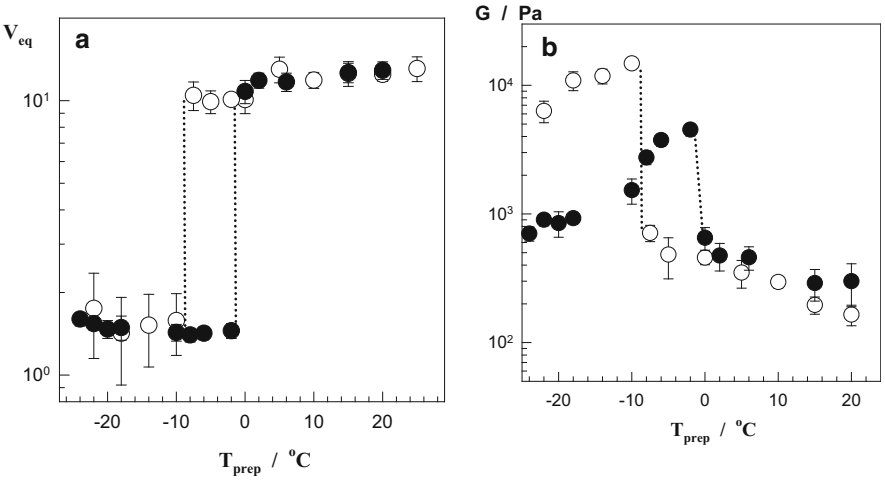

Fig. 11 The equilibrium volume swelling ratio V_{rel} (*left*) and the elastic modulus G of equilibrium swollen PAMPS hydrogels (*right*) shown as a function of T_{prep}. *Filled* and *open symbols* represent data obtained from I- and N-gels, respectively. $X = 1/6$. The *dotted lines* represent the transition temperature. (From [23] with permission of Taylor & Francis Group, LLC)

the reaction solution, the system was immediately cooled down to −196 °C using liquid nitrogen and, then, the system was immersed into a thermostat at $T_{prep} = -2$ °C. The reactions before reaching −2 °C were very slow such that a near isothermal condition was provided. No such precooling step was applied for the preparation of the usual gel sample (N-gel). Although the initial diameters of both gel samples after their preparation were the same (4.3 mm), the swollen volume of N-gel was about tenfold larger than the volume of I-gel. Further, the N-gel was transparent while the I-gel was opaque, both after preparation and after equilibrium swelling in water. The magnified images of the equilibrium swollen gel samples taken with an optical microscope also illustrate the structural differences between the two gel samples (Fig. 10b). Whereas the N-gel was homogeneous in the swollen state, the I-gel exhibited a discontinuous morphology consisting of solvent and gel domains. This means that N- and I-gels prepared at the same T_{prep} are formed in homogeneous gelation and cryogelation regimes, respectively.

In Fig. 11, the equilibrium volume swelling ratio V_{eq} and the modulus of elasticity G of swollen PAMPS gels are shown as a function of T_{prep} [23]. Filled and open symbols represent data points obtained from I- and N-gels, respectively. It is seen that, providing isothermal gelation conditions, the transition temperature shifts from −8 °C to a temperature close to the solvent freezing point (−1 ± 1 °C), as predicted by the simulation results (Fig. 6). Another point shown in Fig. 11 is that the elastic modulus of I-gels prepared below −10 °C is much lower than that of N-gels. This is an indication of the reduced rate of the crosslinking reactions during the formation of I-gels. Thus, the network build-up process seems to take place mainly during the non-isothermal period between 0 °C and T_{prep} so that the I-gels prepared with precooling exhibit a lower modulus of elasticity than the N-gels.

4 Effect of Synthesis Parameters

The properties of cryogels depend on many parameters, including the cryogelation conditions and the composition of the reaction constituents. As the challenge is to control the porous structure and, thus, the cryogel properties, this section focuses on the effect of the synthesis parameters on the morphology of cryogels, with examples selected from the literature.

4.1 Temperature and Freezing Rate

It is known that the size of ice crystals can be controlled by varying the freezing temperature and the freezing rate. For example, to produce large ice crystals, the freezing temperature should be as high as possible and the time for crystallization should be extended. To produce small crystals, freezing should be at a very low temperature and the freezing rate should be high in order to reduce the time available for ice crystals to grow. Because solvent crystals in the cryogelation systems act as templates for the formation of pores, the same relationship usually exists between the pore size of cryogels and the gelation temperature T_{prep} [25, 39, 68]. Because the lower the T_{prep}, the faster the cooling rate of the gelation solution and, thus, the shorter the time period until the freezing temperature of the reaction solution is reached, the T_{prep} and the rate of cooling(or combination of both) do affect the properties of cryogels.

Ivanov et al. investigated the temperature-dependent variation of pore diameter in PAAm cryogels [43]. Cryogels were prepared by crosslinking of linear PAAm chains in aqueous solutions using glutaraldehyde as a crosslinker. It was shown that the pore diameter decreases from 30–60 μm to 10–20 μm as T_{prep} is decreased from −5 to −20 °C [43]. In PAAm cryogels prepared from AAm and BAAm monomers, the largest pore size was obtained at $T_{prep} = -18$ °C and decreased as T_{prep} was further reduced down to −24 °C (Fig. 7d) [26]. The average pore diameters were 60, 32, and 22 μm for $T_{prep} = -18$, −20, and −22 °C, respectively. Similar results were also reported for cryogels derived from aqueous solutions of fibroin chains or DMA monomer (Fig. 12) [28, 50]. In PSA cryogels, the pore diameter decreases from 25 to 11 μm as T_{prep} is decreased from −9 to −20 °C [95]. Since lower T_{prep} means faster freezing of the reaction solution, decreasing pore size with decreasing T_{prep} is consistent with the fact that a larger number of small solvent crystals form as the freezing rate is increased. Additionally, since solvent in large voids is preferentially frozen relative to that in small capillaries due to a smaller freezing-point depression, it is thought that, at T_{prep} close to the solvent freezing point, only solvent in large voids freezes during gelation, leading to large pores. We have to note that there are also conflicting data regarding the temperature dependence of pore size, especially at very low temperatures. This is attributed to the weakness of the cryogel matrices formed at low T_{prep}, which leads to collapse of the porous structure upon drying.

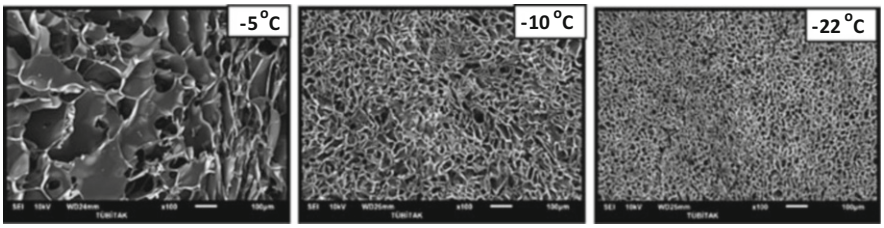

Fig. 12 SEM images of fibroin cryogel networks formed at the various temperatures (T_{prep}) indicated. S*cale bars*: 100 μm. (From [50] with permission from the American Chemical Society)

The formation of polyhedral pores in hydrophilic cryogels may be explained as follows [97, 98]: Water molecules in crosslinked hydrophilic polymers are known to exist in three states: (1) free water in the middle of the mesh of the network, (2) bound water adjacent to the network chains, and (3) film water adsorbed on the bound water layer. Freezing of free water and the growth of ice crystals thus formed may lead to deformation of the polymer network by stretching the hydrated network chains around the ice crystals. Although the polymer elasticity allows easy deformation of the network chains, the high viscosity of the system may slow down growth of the crystals. As a consequence, one may expect formation of ice crystals in the mesh of polymer network separated by swollen polymer chains. Moreover, the total surface energy of ice crystals is minimized by the crystals coming together, forming four ice crystals in contact, with angles of 120° where the forces of interfacial tension balance.

Experiments were also designed to study the effects of freezing rate on the morphology of the cryogels. For this purpose, one part of the reaction solution was slowly frozen in a freezer in contact with air, while the other part was fast frozen in a cryostat in contact with a liquid. The initial cooling rate decreased from 54 to 4 °C/min as the cooling liquid was replaced with cooling air at −18 °C [53]. Figure 13 shows SEM images of the PIB gel network prepared in cyclohexane at $T_{prep} = -10$ °C under fast and slow freezing conditions [53]. It is seen that the size of the pores increases as the freezing rate decreases. Increasing the freezing rate of the reaction solution necessarily reduces the time available for solvent crystals to grow, which would inhibit the formation of large crystals. Thus, small solvent crystals form under fast freezing conditions, which leads to small pores after thawing. Further, increasing the freezing rate shortens the duration of the initial non-isothermal period of the reactions so that the crosslinking mainly occurs in the unfrozen microzones of the apparently frozen reaction system. This may also decrease the size of the pores.

A similar effect of the freezing rate of the gelation solution can be observed by changing the initiator concentration. During the preparation of PSA cryogels in aqueous solutions and using a APS/TEMED redox initiator system, increasing the APS concentration from 1.75 to 3.5 mm decreased the average pore size of the cryogels [95]. This is due to the faster rate of polymerization, which leads to smaller ice crystals. However, further increase in APS concentration decreases the porosity

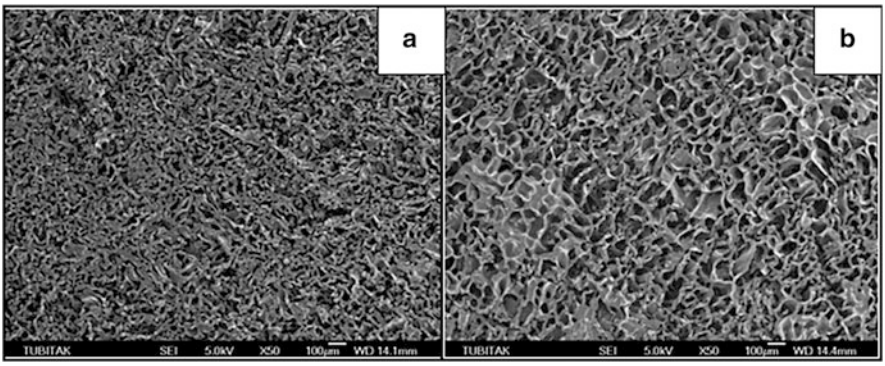

Fig. 13 SEM of PIB networks formed at $T_{prep} = -10$ °C under (**a**) fast and (**b**) slow freezing conditions. Reaction time = 3 days; $S_2Cl_2 = 5.7$ %. *Scale bars*: 100 µm. Magnification 50×. (Reprinted from [53] with permission from Elsevier)

of the cryogels due to the very fast polymerization that occurs before the freezing of the reaction solution. A similar effect of the initiator was also observed in the preparation of PAAm cryogels [25].

The preparation of aligned porous materials with micrometer-sized pores is of particular importance for applications such as tissue engineering, microfluidics, and organic electronics [99, 100]. It was shown that cryogels with an aligned pore structure could be prepared at low freezing rates (i.e., at temperatures close to the transition temperature to the cryogelation regime) or at low polymerization rates (i.e., at a low monomer concentration) [53, 101]. Another requirement is that the solvent used in the reactions should be a solvating diluent for the polymer so that no phase separation takes place during cooling of the gelation solution. For example, during the solution crosslinking of 5 % PIB in cyclohexane, cryogels start to form at or above −2 °C [53]. Moreover, the cyclohexane–PIB system did not show significant temperature effect and, thus, any liquid–liquid phase separation could be prevented during the cryogelation reactions of PIB. SEM images of dried cryogels formed at temperatures T_{prep} close to this upper temperature limit showed an oriented porous structure of the materials [53]. The micrographs in Fig. 14a,b show the alignment of the pores in the gel network formed at $T_{prep} = -2$ °C. The structure consists of brick-shaped pores of about 100 µm in length and 50 µm in width, separated by pore walls of 10–20 µm in thickness. The aligned porous structure of the sample indicates directional freezing of the solvent crystals in the direction from the surface to the interior, i.e., in the direction of the temperature gradient. Note that experiments carried out by decreasing the reactor diameter from 16.4 to 3.7 mm partially destroyed the regularity of the pore structure, probably due to the increasing rate of freezing of the reaction solution. Decreasing the temperature or increasing the cooling rate also destroyed the regularity of the porous structure of the network. The pores of 10–100 µm in size formed at −2 °C became increasingly irregular as T_{prep} decreased [53].

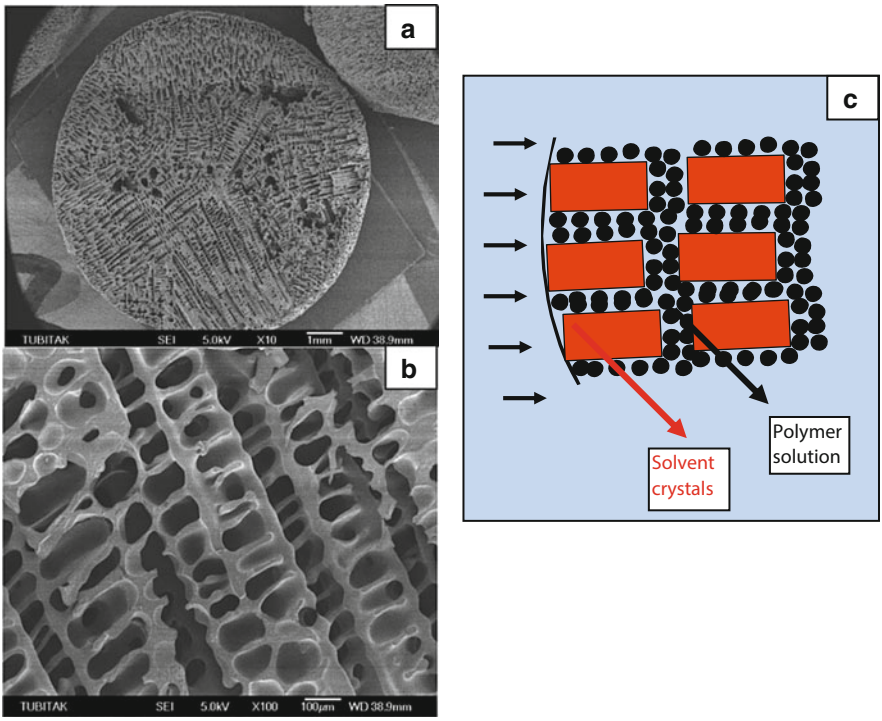

Fig. 14 **(a, b)** SEM of PIB network formed in cyclohexane at $T_{prep} = -2$ °C. Reaction time = 24 h; $S_2Cl_2 = 5.7$ %.**(c)** Scheme showing the directional freezing of PIB solution from the surface to the interior at low cooling rates, i.e., at high T_{prep}. S*cale bars*: 1 mm (**a**), 100 μm (**b**). (Reprinted from [53] with permission from Elsevier)

Because of the poor thermal conductivity of the reaction solution, a temperature gradient is formed in the radial direction and freezing of the solvent cyclohexane starts from the surface of the cylindrical reactor, which is in contact with the cooling liquid at −2 °C. As the solvent freezes, both the PIB chains and the crosslinker S_2Cl_2 are excluded from the solvent crystals due to cryo-concentration and aggregate around the growing crystals to form an unfrozen part of the system. This is illustrated schematically in Fig. 14c. As the freezing progresses, a polymer concentration gradient, as well as a temperature gradient, is established across the moving freezing front. This leads to macroscopic instabilities, due to which the moving freezing front collapses, leaving behind pockets of unfrozen concentrated polymer solution [99, 100]. Further, due to the relatively high T_{prep}, the freezing rate is slow so that the growing solvent crystals can be encapsulated in the concentrated solution and cannot grow further. Thus, directional freezing under a temperature gradient causes crystallization of many isolated solvent crystal phases, leaving an unfrozen gel phase with high polymer content. After the crosslinking reactions, the polymer phase becomes insoluble and, after thawing, preserves the structure that had been conferred to it by the surrounding solvent crystals.

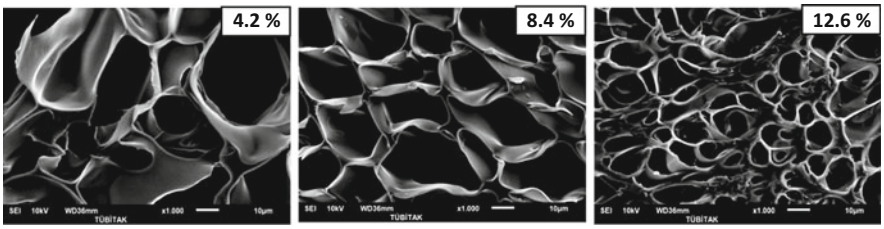

Fig. 15 SEM images of cryogel networks formed at the various fibroin concentrations indicated. S*cale bars*: 10 μm. (From [50] with permission from the American Chemical Society)

4.2 Monomer or Polymer Concentration

It was observed that the architecture or morphology of the cryogel network essentially does not depend on monomer concentration, whereas the size of the structure responds sensitively. In PAAm cryogels, the average pore diameter was found to decrease from 55 to 10 μm with increasing monomer concentration from 3 to 30 % [26]. At the same time, the average thickness of the pore walls increased from 3 to 15 μm. In PAAm cryogels with functional epoxy groups, Plieva et al. also reported decreasing pore size but increasing thickness of pore walls with increasing monomer concentration from 6 to 22 % at $T_{\text{prep}} = -12$ °C [24]. Kirsebom et al. also showed that larger pores and thinner pore walls in poly(DMA) (PDMA) cryogels can be produced from 3 wt% monomer concentration as compared to 12 wt% [28]. In contrast, however, an increasing pore size with increasing concentration was reported for PAMPS hydrogels obtained at $T_{\text{prep}} = -22$ °C [63]. This finding is attributed to collapse of the large pores in such polyelectrolyte gels formed at low monomer concentrations. In cryogelation reactions starting from polymer precursors, increasing the polymer concentration also leads to cryogels with thicker pore walls but a smaller pore size. For instance, at $T_{\text{prep}} = -18$ °C, the pore diameter of fibroin cryogels decreased from 33 ± 10 to 10 ± 3 μm as the fibroin concentration increased from 4.2 to 12.6 % (Fig. 15) [50]. Thus, the higher the monomer (or polymer) concentration, the smaller the pore diameters and the thicker the pore walls [39]. The inverse relation between the precursor concentration and the pore size is related to the higher amount of unfrozen microdomains during gelation as the amount of solute is increased.

4.3 Charge Density

The pore diameters of nonionic PAAm and ionic PAMPS cryogels formed under identical conditions at −22 °C were reported as 100–150 and 30–50 μm, respectively [36]. Thus, the pore size decreases with increasing charge density of the network chains. Calculation results using (8) also predict that an increase in the

charge density *f* of the network chains would decrease the volume fraction of ice in the reaction system so that the pores in the final gels would be smaller [36].

4.4 Crosslinker Concentration

In PAAm and PSA cryogels formed using BAAm crosslinker, no appreciable change in the size of the pores was reported with changes in the crosslinker level [26, 95]. However, in fibroin cryogels formed at $T_{prep} = -18$ °C and in the presence of EGDE as a crosslinker, the average pore diameter decreased from 55 ± 10 to 23 ± 7 μm and the pore-size distribution became narrower as the amount of EGDE increased from 10 to 30 mmol/g [50]. Similar results were reported for rubber cryogels formed using S_2Cl_2 crosslinker. As S_2Cl_2 concentration is increased, both the polydispersity and the average diameter of the pores decrease [52]. This could be due to the increased rigidity of the gel in the unfrozen domains as the amount of crosslinker is increased.

4.5 Additives and Solvent

The presence of low molecular weight salts significantly affects the microstructure of the cryogels formed in aqueous solutions. For instance, addition of NaCl or $CaCl_2$ in aqueous cryogelation solutions results in materials with thicker pore walls and smaller pores [102]. As the NaCl content in the reaction mixture is increased from 0 to 10 % (w/w), the pore size of PAMPS cryogels decreases from 30–50 to 10–20 μm [36]. This is due to the fact that the addition of salts into the reaction system decreases the bulk freezing temperature so that the volume of the nonfrozen solution increases. This leads to the formation of gels with smaller pores. Indeed, as the NaCl content in the reaction mixture is increased from 0 to 10 %(w/v), the bulk freezing times of AMPS-BAAm reaction mixtures at $T_{prep} = -22$ °C increased from 5 to 35 min, whereas their gelation times at 0 °C remained constant (5 ± 1 min) [36]. Moreover, addition of a polymerization inhibitor such as hydroquinone into the reaction solution produces more monodisperse and smaller pores in PAAm cryogels [23]. Hydroquinone provides homogeneous nucleation of ice crystals due to the shift of the gel point beyond freezing of the reaction solution, so that the number of crystals increases while their size decreases, leading to the formation of small pores in PAAm cryogels.

The addition of micro- or nanoparticles in the cryogelation system produces hybrid cryogels with increased modulus of elasticity [56, 103–106]. For instance, such cryogels were prepared by the addition of tetramethoxysilane in aqueous solutions of PVA before its freeze–thaw treatment [104]. They can also be prepared by crosslinking of PIB in cyclohexane containing silica nanoparticles and using S_2Cl_2 as a crosslinking agent [56]. The microstructure of the hybrid PIB cryogels

consists of two types of pores: 10^1 μm large pores due to the cyclohexane crystals acting as a template during gelation and 10^{-1}–10^0 μm small pores between the aggregates of the nanoparticles. The nanoparticles in hybrid cryogels accumulate within the large pores where cyclohexane crystals originally resided. The cryogels exhibit a 300-fold larger modulus of elasticity than those prepared in the absence of nanoparticles [56]. It was shown that these hybrid cryogels can be converted into organic cryogels by dissolving the silica component in aqueous hydrofluoric acid, whereas removing the polymer component by calcination results in porous silica networks with 10^{-1}-μm-sized pores [56].

The internal morphology of cryogels is also dependent on the type of solvent used in cryogelation reactions. This effect arises due to the different shape of solvent crystals as well as due to the temperature-dependent variations of the interactions between the polymer and solvent. For instance, PAAm cryogels prepared in formamide at −20 °C have an oriented porous structure with long pores as a result of the formation of needle-like formamide crystals [25]. Moreover, in contrast to the interconnected 3D pore structure of PNIPA cryogels formed in water, those formed in dioxane/water medium have a closed pore structure with thick (10–40 μm) pore walls [33]. The effect of polymer–solvent interactions on the morphology of cryogels can be illustrated using PIB cryogels formed in cyclohexane and in benzene under identical conditions. Besides their molecular sizes, benzene and cyclohexane have similar freezing and melting properties; they both form high temperature orientationally disordered crystals and their melting temperatures in the bulk are close (5.5 versus 6.5 °C for benzene and cyclohexane, respectively) [107]. However, since the chemical structure of cyclohexane is close to that of the repeating unit of polyisobutylene, it is a good solvent for PIB. In contrast to cyclohexane, benzene is a poor solvent for PIB and becomes poorer as the temperature decreases [53]. SEM images of PIB networks formed in benzene and in cyclohexane show different morphologies. In contrast to the regular morphology of the cryogels prepared in cyclohexane, those formed in benzene exhibit a broad size distribution of pores from micrometer to millimeter sizes [52]. Further, the total volume of pores V_p in PIB gels formed in benzene was found to increase from 6 to 9 mL/g as T_{prep} is decreased from −2 to −18 °C, in contrast to the value of about 2.5 mL/g for all low-temperature gels formed in cyclohexane [52, 53]. The differences observed in the morphology of the gels are due to the cooling-induced phase separation of the PIB chains in benzene [52]. Thus, the gel cannot absorb all the available solvent during gelation so that a macrophase separation should occur during the initial non-isothermal period of the reactions.

If the cryogelation reactions are conducted in a good solvent/poor solvent mixture, the mechanism of pore structure formation by cryogelation can be combined with the reaction-induced phase separation. For instance, PAAm cryogels formed at −12 °C in acetone–water mixtures exhibit two types of pores [102]. The 10–80 μm large pores are due to the ice crystals acting as a template during gelation while the submicrometer-sized pores in the pore walls are due to the χ-induced phase separation in the unfrozen phase enriched with acetone (a poor solvent for PAAm) and the monomers [102]. Another interesting example is PAAm cryogels

prepared at −18 °C in aqueous DMSO solutions of various compositions [59]. DMSO–water mixtures exhibit a marked freezing point depression and the reaction system will freeze at −18 °C if the DMSO content is less than about 30 % (v/v). Indeed, the hydrogels formed in the solvent mixture with less than 30 % DMSO by volume have irregular large pores of about 10^1 μm in diameter, typical for macroporous networks created by the cryogelation technique. Nonporous hydrogels were obtained in solutions containing 25 % DMSO, while at larger DMSO contents the structure of the hydrogel networks consists of aggregates of microspheres that look like cauliflowers, as typical for a macroporous network formed by a reaction-induced phase separation mechanism [59]. The results were interpreted as a transition from cryogelation to phase separation copolymerization due to the marked freezing point depression of the solvent mixture, as well as due to the action of the mixed solvent as a poor solvating diluent at −18 °C [59].

5 Novel Cryogels and Their Applications

In this section, some novel cryogel materials based on DNA, silk fibroin, poly (acrylic acid), and several types of rubber are presented, and their applications in various fields are summarized.

5.1 DNA Cryogels for Removal of Carcinogenic Agents

Deoxyribonucleic acid (DNA) serves as the carrier of genetic information in living organisms and is composed of building blocks called nucleotides, which consist of deoxyribose sugar, a phosphate group, and four bases (adenine, thymine, guanine, and cytosine). DNA has a double-helical (ds) conformation in its native state, which is stabilized by hydrogen bonds between the bases attached to the two strands [108]. When a DNA solution is subjected to high temperatures, the hydrogen bonds holding the two strands together break and the double helix dissociates into two single strands (ss) having a random coil conformation [109]. Due to its unique ds-structure, DNA has highly specific functions, such as intercalation, groove-binding interactions, and electrostatic interactions. These functions are specific for DNA molecules and are difficult to reproduce in synthetic polymers. Although films and fibers can be prepared from DNA, such materials are water soluble, biochemically unstable, and mechanically weak.

A DNA hydrogel is a network of chemically crosslinked DNA strands swollen in aqueous solutions [110–112]. Such soft materials are good candidates for making use of characteristics of DNA such as coil–globule transition, biocompatibility, selective binding, and molecular recognition [113, 114]. DNA hydrogels can be prepared by crosslinking of DNA in aqueous solutions at 50 °C using diepoxides such as EGDE or BDDE as chemical crosslinking agents [112, 115]. The reaction

between epoxides and DNA is of nucleophilic substitution type (S_N2 reaction) and occurs at the nucleophilic sites in DNA, mainly at the N7 position of guanine. DNA hydrogels are responsive systems that exhibit drastic volume changes in response to external stimuli, such as acetone [115], poly(ethylene glycol) [112], inorganic salts [116, 117], polyamines [117], cationic macromolecules [118], or surfactants [117]. Responsive DNA hydrogels with a wide range of tunable properties, such as the conformation of the network strands, viscoelasticity, and nonlinear elasticity (strain hardening), have been prepared in the past few years [111, 112, 119].

Recently, DNA cryogels with excellent mechanical properties have been obtained by conducting gelation reactions at subzero temperatures [47, 48]. DNA cryogels were prepared at $T_{prep} = -18$ °C from frozen aqueous solutions of ds-DNA (about 2,000 base pairs long) containing BDDE crosslinker and TEMED catalyst. Infrared (IR) and fluorescence measurements show the predominantly ds-DNA conformation of the network chains of DNA cryogels. An almost complete conversion of soluble to crosslinked DNA required 3 % DNA and 0.39 % BDDE, corresponding to the presence of an equimolar ratio of epoxy to DNA base pair in the gelation solutions [48]. DNA cryogels exhibited weight swelling ratios (q_w) between 40 and 130, indicating that they are in a highly swollen state with 98–99 % water in the cryogel structure. However, their volume swelling ratios q_v are about one order of magnitude smaller than their weight swelling ratios q_w. The total porosity P_s of the cryogels estimated from their q_w and q_v values using (4) is 93–99 % for all the cryogels. The total volume of the pores V_p in the cryogels, estimated from the uptake of methanol, is between 3 and 20 mL/g, indicating that the total pore volume of the cryogel samples is much larger than the bulk gel volume. This suggests that most of the water in swollen cryogels is within the pores, while the crosslinked DNA forming the pore walls is less swollen. Mechanical tests show that the cryogels formed at 5 % DNA are very tough and can be compressed up to about 80 % strain without any crack development [48]. They also exhibit completely reversible swelling–deswelling cycles in response to solvent changes.

Carcinogenic agents having planar aromatic groups can intercalate into DNA double helices, which means that DNA can be used to prepare selective and efficient adsorbents of such specific toxic agents. It was shown that DNA cryogels can be used for the removal of such toxic agents from aqueous solutions [47, 48]. This is exampled by use of the classical intercalator ethidium bromide (EtBr), which is a four-ringed aromatic molecule with three of the rings conjugated. The nature of the interaction of EtBr with DNA has been examined by a variety of techniques over the past 50 years [120–123]. It is generally recognized that the strong mode of binding of EtBr to ds-DNA results in the intercalation of the planar phenanthridium ring between adjacent base pairs on the double helix. The intercalation of EtBr both increases the distance between base pairs by 0.3 nm and unwinds the double helix by 26°, which causes an increase in length of the DNA [124, 125]. Moreover, at high concentrations, EtBr also interacts with DNA by electrostatic interactions.

Figure 16a shows the EtBr concentration in the external solution ($C_{f,t}$) plotted against the contact time t with DNA cryogels [48]. For comparison, the behavior of

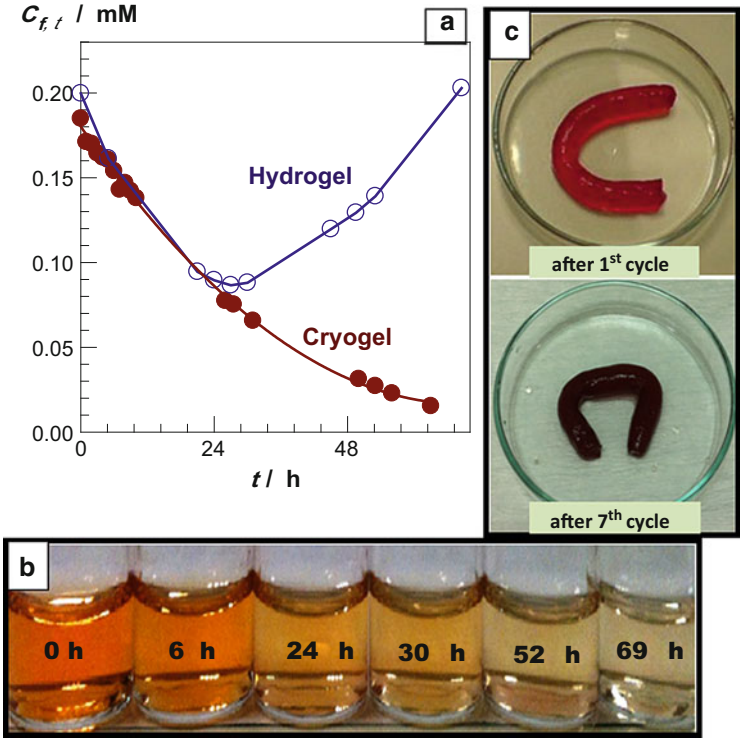

Fig. 16 (**a**) EtBr concentration ($C_{f,t}$) in the external solution plotted against the contact time t with the cryogel and hydrogel of DNA. (**b**) Images of the external EtBr solution at various times during the first absorption cycle using DNA cryogel. (**c**) Images of DNA cryogel after the first and seventh absorption cycles. (From [48] with permission from Elsevier)

DNA hydrogels prepared by usual gelation process is also shown. The initial EtBr concentration in the solution is 0.2 mM. During the first 24 h, $C_{f,\,t}$ decreases with almost the same rate, and both gel samples bind 0.10–0.15 mol EtBr per mole of nucleotide. At longer times, the hydrogel sample starts to disintegrate, as can be seen in Fig. 16 from the increase in EtBr concentration. After about 3 days, DNA hydrogel completely dissolved in EtBr solution (see below for explanation). In contrast, the DNA cryogel remained stable over the whole time period while continuously absorbing EtBr, during which time the color of the solution changed from red to clear (Fig. 16b). This highlights the stability of DNA strands in the cryogels and, thus, demonstrates that DNA cryogels are effective sorbents as compared to DNA hydrogels. The cryogel samples subjected to nine successive sorption cycles in 0.2 mM EtBr solutions also remained stable in aqueous solutions. As can be seen in Fig. 16c, the color of the cryogel changes from clear to red during the first cycle and becomes dark red after seven cycles, revealing an increasing amount of bound EtBr in the cryogel.

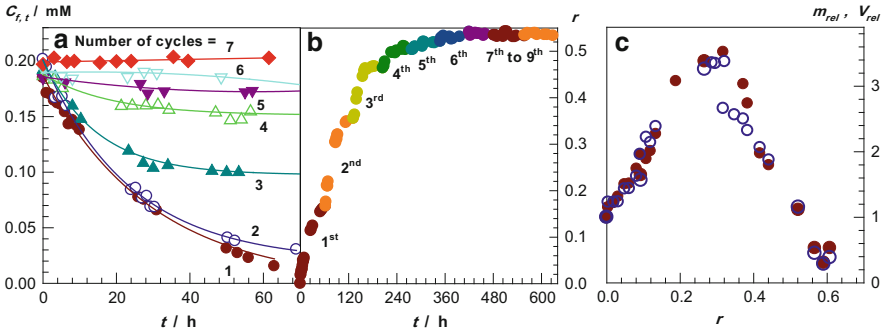

Fig. 17 **(a)** EtBr concentration ($C_{f,\,t}$) plotted against the contact time t for DNA cryogels. The results of seven successive sorption cycles are shown. **(b)** EtBr bound per nucleotide r plotted against the cumulative contact time t of nine successive cycles. **(c)** Relative gel mass m_{rel} (*filled symbols*) and volume V_{rel} (*open symbols*) of DNA cryogels shown as a function of r. (From [48] with permission from Elsevier)

The results of seven successive sorption cycles are shown in Fig. 17a, where $C_{f,\,t}$ is plotted against the contact time with the DNA cryogel. During the first two cycles, EtBr concentration decreases from 0.2 mM to about 0.02 mM, i.e., 90 % of the EtBr in the solution is absorbed by the cryogel. The sorption capacity decreases in the following cycles and the cryogel saturates after six cycles. In Fig. 17b, the number of EtBr molecules bound per nucleotide (denoted by r) is plotted against the cumulative contact time of successive cycles. A rapid sorption of EtBr by the cryogel up to r =0.45, followed by a slow sorption process, can be seen from the figure. Repeated tests showed that the total capacity of the cryogels is 0.6 ± 0.1 EtBr molecules per nucleotide. Since the maximum amount of EtBr that can bind to DNA is one molecule per base pair, the results show that this value can be achieved using cryogels without disturbing the integrity of the gel structure.

The swelling behavior of the cryogels depending on the amount of bound EtBr per nucleotide is illustrated in Fig. 17c [48]. Here, the normalized cryogel mass m_{rel} and volume V_{rel} with respect to those in pure water are shown as a function of r. At low ratios of bound EtBr to DNA ($r < 0.3$), the gel swells with increasing amount of bound EtBr. After a 3.5-fold increase in the volume and mass of the gel at $r = 0.3$, it starts to deswell again and finally attains a compact mass at $r = 0.6$. The equality of mass and volume changes of the cryogels demonstrates that this unusual swelling behavior is related to the gel structure, but not the porosity changes depending on EtBr binding.

To understand the unique swelling behavior of DNA cryogels in EtBr solutions, one has to consider the nature of interactions of EtBr with nucleic acids in aqueous solutions. Previous studies indicate the existence of two main types of EtBr binding to DNA [121, 122]. At low values of r, EtBr binds strongly to DNA sites by intercalation, which appears to be saturated when one EtBr molecule is bound for every 2.1 ± 0.2 base pairs, i.e., $r = 0.24 \pm 0.02$. This is the accepted maximum

value for intercalation based on the neighbor exclusion model. Sorption of EtBr by the cryogels with 90 % efficiency, observed at $r < 0.25$, is thus attributed to the intercalation of EtBr within the double helical DNA strands. Moreover, the intercalation of EtBr into DNA changes the rotation angle between adjacent base pairs and unwinds the helix, resulting in lengthening of the DNA strand [124, 125]. This process also increases the viscosity of DNA solutions due to the increasing hydrodynamic size of DNA strands [126]. The extent of the increase in viscosity depends on the number of EtBr molecules bound per nucleotide; this behavior is also a characteristic of all DNA intercalators. Thus, the initial swelling of DNA gels at $r < 0.3$ may originate from the increasing length of DNA network chains, which decreases the elastically effective crosslink density of the cryogels. We should mention that the disintegration of DNA hydrogels at $r = 0.10$–0.15 could also be related to this phenomenon (Fig. 16a). Lengthening and stiffening of the helix due to intercalated DNA decreases the crosslink density of the hydrogels [48], leading to their dissolution in EtBr solutions. In contrast, cryogels are stable in EtBr solutions due to the dense pore walls formed during cryo-concentration.

The swelling response of DNA cryogels to changes in EtBr concentration between 3 and 300 μM also suggests that they can be used to detect DNA-binding substrates in aqueous solutions. On the other hand, it was reported that at high r ratios ($r > 0.25$), after the primary sites of DNA have been filled, a secondary binding process occurs arising from electrostatic interactions between phosphate residues and EtBr molecules attached outside the helix. As a consequence, in this range of r, the cryogel deswells with increasing concentration of EtBr, which is similar to the behavior of polyelectrolyte hydrogels immersed in aqueous solutions of increasing salt concentration. The results thus show that DNA cryogels can be used as a specific sorbents to remove carcinogenic agents from aqueous solutions. Moreover, the response of DNA cryogels to changes in EtBr concentration between 3 and 300 μM also suggests that they can be used to detect DNA-binding substrates in aqueous solutions.

5.2 *Fibroin Cryogels as Mechanically Strong Scaffolds*

Silk fibroin derived from *Bombyx mori* is a fibrous protein exhibiting extraordinary material properties such as good biocompatibility, biodegradability, high strength and toughness, and ease of processability [127–129]. Silk fibroin has been used for cell culture, wound dressing, drug delivery, enzyme immobilization, and as a scaffold for bone tissue engineering [130, 131]. Silk fibroin has a blocky structure consisting of less-ordered hydrophilic blocks and crystallizable hydrophobic blocks [132–135]. Hydrophilic blocks provide solubility in water and are responsible for fibroin elasticity and toughness, whereas hydrophobic blocks form intermolecular β-sheet structures leading to the insolubility and high strength of fibroin. Several techniques have been developed to produce porous fibroin scaffolds such as freeze–thawing, porogen leaching, gas foaming, electrospinning, and freeze-drying

[136–146]. The principle of the porogen leaching and gas foaming techniques is the use of porogens, such as sodium chloride and ammonium percarbonate acting as a template and gas-forming agent, respectively. After treatment of fibroin/porogen composites with alcohols to induce β-sheet formation, the porogen is leached out with water to form the pores of the scaffolds. To produce fibroin scaffolds by freeze-drying, aqueous fibroin solutions are mixed with alcohol to obtain a gel precipitate following freezing at a low temperature, and are finally freeze-dried [137]. It was shown that the porogen leaching and gas foaming techniques produce scaffolds having larger pores (100–200 μm) than the scaffolds formed by freeze-drying (10–50 μm). The compressive moduli of the scaffolds vary, depending on the preparation conditions between 10 kPa and 3 MPa.

An alternative simple route for the production of 3D highly porous fibroin networks is the cryogelation technique. Silk fibroin cryogels with remarkable properties were recently obtained from frozen fibroin solutions (4.2–12.6 %) at subzero temperatures between −5 and −22 °C [50]. This was achieved by the addition of EGDE to the cryogelation system. It was shown that the cryogelation reactions conducted in the absence of EGDE did not lead to gel formation after 1 day of reaction time, indicating that cryo-concentration alone does not induce fibroin gelation. Experiments indicate that the presence of EGDE triggers the conformational transition of fibroin from random coil to β-sheet structure and, hence, fibroin gelation [49, 50]. Figure 18a shows the amide I band region of ATR-FTIR spectra, presenting the carbonyl stretching vibration of amide groups on silk fibroin. The spectrum of fibroin before gelation (dotted curve in Fig. 18a) is characterized by a peak at 1,640 cm^{-1}, which indicates the presence of primarily random coil and/or β-helix conformations [147, 148]. After cryogelation, all samples display a main peak at 1,620 cm^{-1}, which was assigned to the β-sheet conformation [148]. In addition to the main peak, shoulders at 1,660 and 1,698 cm^{-1} are seen, which can be assigned to α-helix and β-turn conformations, respectively. This indicates the occurrence of a conformational transition from random coil to β-sheet structure in frozen fibroin solutions. Further evidence for the β-sheet formation comes from the X-ray profiles of freeze-dried cryogels (Fig. 18b). Silk fibroin before gelation (dotted curve in Fig. 18b) exhibits a broad peak at around 22^{o}, indicating an amorphous structure [149]. After gelation, all the cryogels show a distinct peak at 20.9^{o} and two minor peaks at 9.8 and 24.5^{o}. These are the characteristic peaks of the β-sheet crystalline structure of silk fibroin, corresponding to β-crystalline spacing distances of 4.3, 9.0, and 3.6 A^{o}, respectively [149, 150]. The results of β-sheet content analysis show that fibroin chains before gelation have 12 ± 2 % β-sheet structures, while their contribution increases to 33 ± 2 % [50].

One of the unique features of fibroin cryogels is their elasticity, which allows them to resist compression without any crack development. All the cryogel samples were very tough and could be compressed up to about 99.8 % strain without any crack development; during compression, water inside the cryogel was removed (Fig. 9). Upon unloading, the compressed cryogel immediately swelled to recover its original shape.

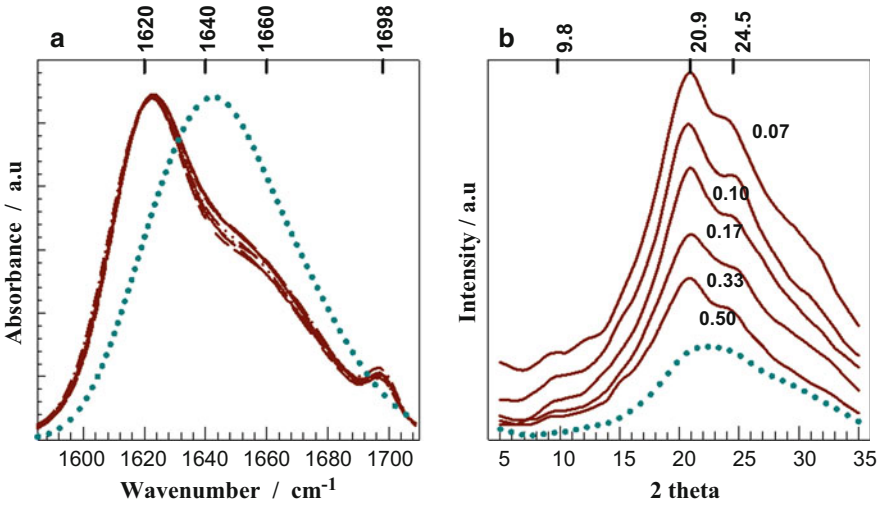

Fig. 18 Amide I region of (**a**) FTIR spectra and (**b**) X-ray diffraction profile of freeze-dried fibroin cryogels. Data obtained by freeze-drying of silk fibroin solutions before gelation are also shown (*dotted curves*).(**a**) TEMED content (%): 0.07 (*solid curve*), 0.10 (*long dash*), 0.13 (*short dash*), 0.17 (*short-long*), 0.25 (*dash-dot-dot*), 0.33 (*short-long-short*), and 0.50 % (*dash-dot*). (**b**) TEMED content (%) is indicated on the curves. $T_{prep} = -18$ °C; $C_{SF} = 4.2$ wt%; EGDE = 20 mmol/g. (From [50] with permission from the American Chemical Society)

It was shown that the critical stress σ_p corresponding to the plateau regime in the stress–strain curves of cryogel scaffolds increases with decreasing pore diameter, that is, with decreasing gelation temperature T_{prep} or with increasing fibroin or EGDE concentrations [50]. Figure 19a shows the stress–strain curves of cryogel scaffolds formed at $T_{prep} = -18$ °C and at three different fibroin concentrations C_{SF}. Inspection of the curves reveals that the critical stress σ_p increases from 0.6 to 4.4 MPa with increasing fibroin concentration C_{SF} from 4.2 to 12.6 %, i.e., with decreasing pore diameter from 33 to 10 μm (Fig. 15). The results suggest an increasing mechanical stability of the porous structure of fibroin scaffolds with decreasing size of the pores. Indeed, the compressive modulus and the compressive stress measurements of the scaffolds support this finding. The cryogel scaffolds formed at $T_{prep} = -18$ °C and $C_{SF} = 4.2$ % exhibit a compressive modulus E of 8 ± 1 MPa, with a compressive nominal stress σ_{comp} of 0.22 ± 0.04 MPa. These values are about one order of magnitude higher than those of the hydrogel scaffolds formed at $T_{prep} = 50$ °C. As illustrated in Fig. 19b, the modulus E and the compressive stress σ_{comp} further increase to 48 and 1 MPa, respectively, as C_{SF} is increased from 4.2 to 12.6 %.

We have to mention that fibroin scaffolds formed by freeze-drying of fibroin solutions pretreated with alcohols exhibit compression moduli of 10–100 kPa, whereas the salt leaching method generates scaffolds with a modulus of 0.5 MPa [137]. The largest compressive modulus and compressive strength reported so far

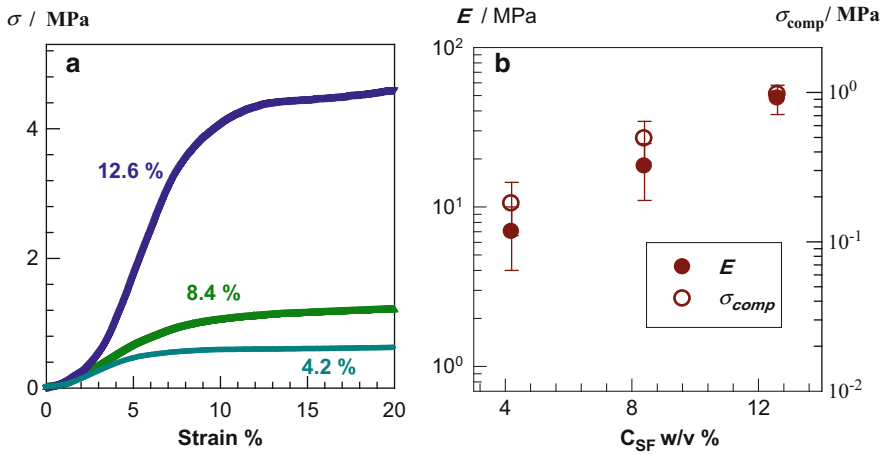

Fig. 19 **(a)** Stress–strain curves of fibroin scaffolds formed at various C_{SF}, shown as the dependence of the nominal stress σ on the degree of compression. C_{SF} as indicated in the figure; $T_{prep} = -18$ °C; EGDE = 20 mmol/g; TEMED = 0.25 %. **(b)** The compressive modulus E and compressive stress σ_{comp} of fibroin scaffolds are shown as a function of fibroin concentration C_{SF} in the feed. $T_{prep} = -18$ °C; EGDE = 20 mmol/g; TEMED = 0.25 %. (From [50] with permission from the American Chemical Society)

for fibroin scaffolds are 3 MPa and 60 kPa, respectively, which were for gels produced by the gas foaming technique [137]. Thus, as compared to other techniques, cryogelation conducted at $T_{prep} = -18$ °C and using 12.6 % fibroin in the feed leads to fibroin scaffolds exhibiting 16-fold larger modulus and strength (48 ± 10 MPa and 970 ± 50 kPa, respectively). The extraordinary strength of the cryogel scaffolds originates from the high fibroin concentration of the pore walls; gelation in frozen solutions confines the fibroin in a small region of the reaction volume, forming the pore walls of the final material. This also provides a high degree of toughness to cryogels in their swollen states.

5.3 *Poly(Acrylic Acid) Cryogels as Self-Oscillating Systems*

Conventional responsive hydrogels either swell or deswell in contact with external stimuli, that is, they make only a single action in response to external variables. In contrast, however, the so-called self-oscillating hydrogels exhibit swelling–deswelling cycles in contact with a solution [151]. Thus, self-oscillating hydrogels create dynamic rhythms and may open new application areas such as self-walking microactuators or micropumps with peristaltic motion, pacemakers, timers, and oscillatory drug release systems [151].

Self-oscillating hydrogel systems can be designed by coupling a responsive hydrogel sample with oscillating chemical reactions. For example, the Belousov–Zhabotinsky (BZ) reaction is a well-known oscillating system and the overall process of the reaction is the oxidation of a substrate such as malonic acid in the presence of oxidizing agent (bromate) and metal catalyst in an acidic solution [152, 153]. Yoshida and coworkers used poly(*N*-isopropyl acrylamide) gel in a BZ reaction to produce a self-oscillating gel system [151, 154]. Crook et al. used poly(methacrylic acid) (PMAAc) gel in a Landolt oscillating reaction system consisting of bromate, sulfite, and ferrocyanide ions [155, 156]. Although the actual mechanism of this bromated oscillation system is complicated, the overall reaction consists of two main steps: (1) the oxidation of sulfite by bromate and (2) the oxidation of ferrocyanide by bromate, i.e., [155]:

$$BrO_3^- + 3HSO_3^- + H^+Br^- + 3SO_4^{2-} + 4H^+ \tag{11a}$$

$$BrO_3^- + 6Fe(CN)_6^{4-} + 6H^+Br^- + 6Fe(CN)_6^{3-} + 3H_2O \tag{11b}$$

Thus, the first reaction produces H^+ ions so that pH of the reaction solution decreases, while the second reaction consumes H^+ ions so that the pH again increases. In response to the oscillatory pH changes in solution, a weak polyelectrolyte gel such as PMAAc oscillates between swollen and collapsed states.

However, all of the self-oscillating conventional hydrogels are limited in their size to microscopic dimensions, due to their slow rate of response to external stimuli. Recently, it was shown that centimeter-sized poly(acrylic acid) (PAAc) cryogels can be used as a pH oscillator in oscillatory bromate–sulfite–ferrocyanide reactions [31]. The cryogels were prepared at −18 °C from frozen aqueous solutions of acrylic acid (AAc) monomer and BAAm crosslinker. Fast responsive macroporous PAAc cryogels could be obtained at an initial monomer concentration C_o of ≤4 % (w/v). In Fig. 20, the diameter D of PAAc cryogels formed at $C_o = 2$ % is shown as a function of time during three successive deswelling–reswelling cycles in methanol and water, respectively. The gel diameter D varies between 8 and 2 mm, i.e., the gel exhibits completely reversible cycles. This 64-fold change in the gel volume during the swelling–deswelling cycles does not induce any crack formation, and the network structure remains stable. The results thus suggest that such gel samples are useful materials in oscillating reaction systems.

Indeed, PAAc cryogels coupled with a bromate oscillator oscillated between swollen and collapsed states [31]. The reactions of bromate, sulfite, and ferrocyanide ions were conducted in an open continuously stirred tank reactor. Four feed solutions (potassium bromate, sodium sulfite, potassium ferrocyanide, and sulfuric acid) were supplied continuously to the reactor, during which the pH of the reaction solution was monitored as a function of time. The flow rate of the feed solutions is an important parameter in determining the extent of pH oscillations. In Fig. 21, pH versus time plots are shown for four different reduced flow rates k, defined as the flow rate of the feed solutions divided by the reaction volume. It is seen that the pH of the solution oscillates between 6.2–6.9 and 3.2–3.8. The dissociation degree α of a weak electrolyte relates to pH by:

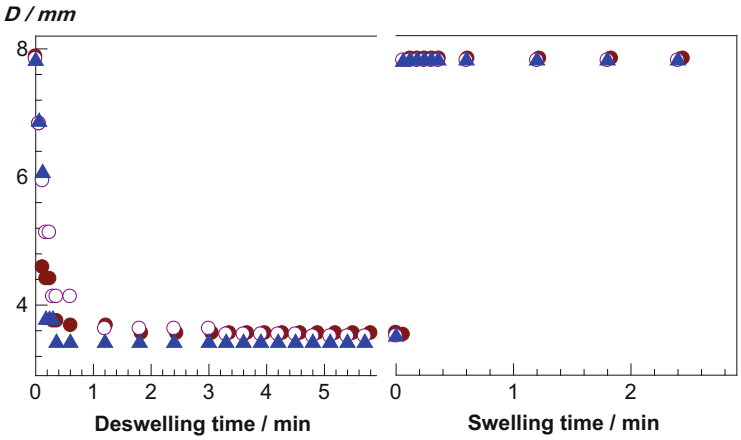

Fig. 20 Deswelling–reswelling kinetics of PAAc cryogels formed at 2 % initial monomer concentration are shown as the variation in gel diameter D with time. The data points are results of the measurements during the first (*filled circle*), second (*open circle*), and third (*filled triangle*) deswelling–reswelling cycles. (From [31] with permission from John Wiley & Sons)

$$\mathrm{pH} = \mathrm{p}K_\mathrm{a} + \log\left(\frac{\alpha}{1-\alpha}\right) \tag{12}$$

Using $\mathrm{p}K_\mathrm{a} = 4.25$, as reported for PAAc gels [157], one may calculate the dissociation degree α as 0.15 and 0.99 for pH values of 3.5 and 6.5, respectively. Thus, if PAAc gel is immersed into this solution, the concentration of the mobile ions (Na^+) inside the gel will change sevenfold during these pH oscillations. Figure 21 also shows that the larger the flow rate k, the larger the extent of oscillation. Furthermore, increasing flow rate also increases the time period at high and low pH values. For example, at $k = 1\times10^{-4}$ and 1×10^{-3} s^{-1}, the pH of the solution remains above pH 6 for 25 and 75 min in each cycle, respectively. The results in Fig. 21 also demonstrate that the oscillation proceeds monotonically with fixed values of the maximum and minimum pH.

Figure 22 demonstrates the behavior of PAAc cryogels in this pH oscillating system. Here, the pH and the gel diameter D are plotted as a function of time at a flow rate $k = 5\times10^{-4}$ s^{-1}. Gel samples of 5 mm in diameter and about 1 cm in length (approximately 1 cm^3) were used in the experiments. Images of the gel samples were taken every minute using an image analyzing system, while the pH of the solution was also monitored by PC. The images in Fig. 22 were taken from the gel sample in swollen and collapsed states. It is seen that, depending on the pH oscillations, the diameter of the gel sample periodically varies between 7 and 5 mm, indicating a threefold change in the gel volume.

At high pH, the concentration of the mobile ions inside the PAAc cryogel increases (12) so that the difference between the mobile ion concentration inside

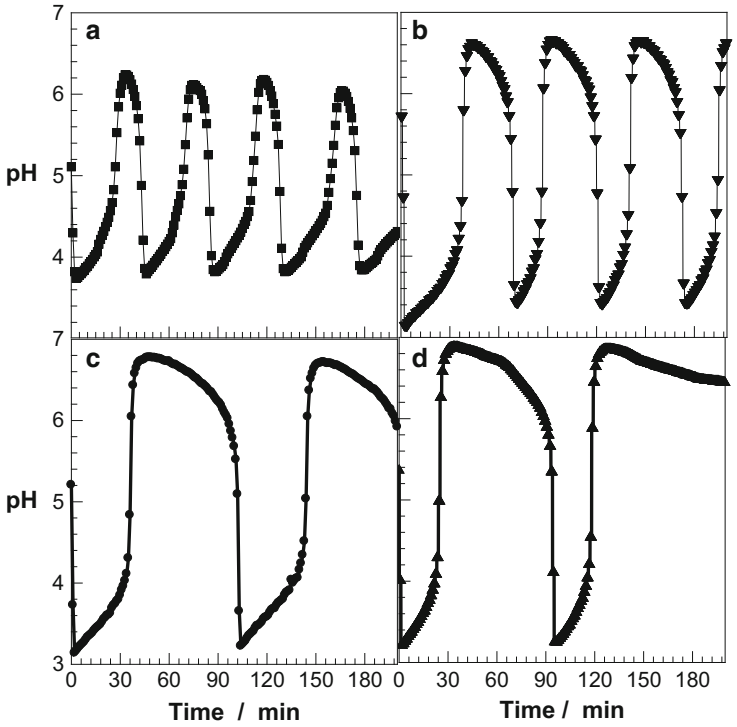

Fig. 21 (**a**–**d**) pH of the reaction solution shown as a function of time. Flow rate $k = 1\times10^{-4}$ (**a**), 2×10^{-4} (**b**), 3.5×10^{-4} (**c**), and 10×10^{-4} s^{-1} (**d**). (From [31] with permission from John Wiley & Sons)

and outside the gel rises, which creates additional osmotic pressure that expands the gel. The opposite behavior occurs at low pH, which induces deswelling of the gel sample. However, the extent of volume change in the pH oscillating reaction is much smaller than that observed in swelling–deswelling experiments, as shown in Fig. 20. This is due to the high salt concentration in oscillating reaction systems, which partially screens the charge interactions within the cryogel.

The results thus show that PAAc cryogels produce periodic swelling–deswelling oscillations in the bromate oscillation system. As the response rate of cryogels does not depend on their size, much larger cryogel samples can also be used in self-oscillating systems. This suggests that, like the back-and-forth motion of a piston of a heat engine, a pH-responsive cryogel could be used as a working substance to convert random molecular energy into macroscopic mechanical energy of lower entropy.

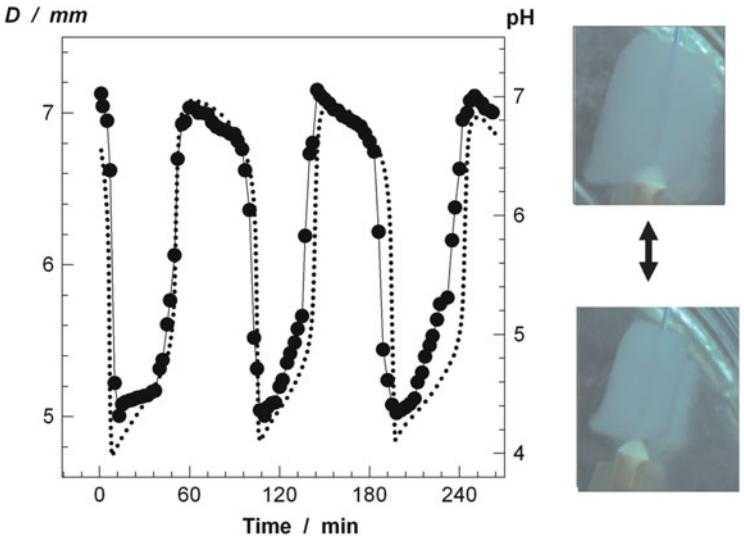

Fig. 22 Variations in pH (*dotted curves*) and gel diameter D (*symbols*) as a function of time. Flow rate $k = 5\times10^{-4}$ s^{-1}. The pictures on the *right* show the gel samples at high and low pH. (From [31] with permission from John Wiley & Sons)

5.4 Rubber Cryogels as Reusable Oil Sorbents

Accidents involving oil tankers can result in the release of large volumes of crude oil, and this risk significantly increases along narrow seaways with heavy maritime traffic. Removal of crude oil and petroleum products that are spilled at sea has been a serious problem in recent decades [158]. Among existing techniques for the removal of oil, the use of sorbents is generally considered to be one of the most efficient techniques [159, 160]. The properties of an ideal sorbent material for oil spill cleanup include hydrophobicity, high uptake capacity and high rate of uptake, buoyancy, reusability or biodegradability, and recoverability of oil. Although several materials have been proposed as sorbents for oil removal, polymeric materials based on nonwoven polypropylene are the most commonly used commercial sorbents in oil spill cleanup [161–165]. However, commercial oil sorbents are not reusable, meaning that they form a solid waste after the cleanup procedures.

The reusability of the sorbents and the recoverability of the crude oil are important aspects of oil spill cleanup procedures. Because cryogels are squeezable gels and the liquid in the cryogels can simply be recovered via manual hand compression, hydrophobic cryogels are good candidates as oil sorbents for oil spill removal. The most suitable polymeric precursor for the preparation of cryogels as sorbent for crude oil can be estimated using the solubility parameters. According to the Hildebrand theory [166], the solvating (swelling) power of a polymer–solvent medium can be estimated from $(\delta_1-\delta_2)^2$, where δ_1 and δ_2 are the solubility

parameters for the solvent and the polymer, respectively. The solubility of a polymer in a solvent is favored when $(\delta_1-\delta_2)^2$ is minimized, i.e., when the solubility parameters of the two components are most closely matched. The value of δ_1 for aliphatic and some aromatic hydrocarbons, as a model for crude oil, is close to the δ_2 of rubbers such as PIB, CBR, and SBR (16.5–16.8, 18.0, and 18.1 $MPa^{1/2}$, respectively) [51, 167, 168]. As a consequence, crude oil is a good solvent for these rubbers and can be used for the production of cryogels for use as oil sorbents.

As detailed in Sect. 2.1, the dilute solutions of rubbers such as PIB, SBR, and CBR can be crosslinked using sulfur monochloride (S_2Cl_2) as a crosslinking agent. Experiments show that S_2Cl_2 is an efficient crosslinking agent in organic solutions such as benzene or cyclohexane, even at very low reaction temperatures down to −22 °C and at crosslinker ratios down to about 0.9 mol S_2Cl_2/mol internal vinyl group on the rubber [52, 53, 55]. The reaction between S_2Cl_2 and the unsaturated groups of the rubbers PIB, CBR, and SBR in frozen organic solutions is due to the effect of cryo-concentration below the freezing point of the solvent. For instance, when a 5 % (w/v) PIB solution in benzene is frozen at −18 °C, 14 % of the benzene remains unfrozen in the apparently frozen system, making the PIB concentration in the unfrozen regions about 36 %, which is high enough to conduct the crosslinking reactions even at −18 °C [52].

Figure 23 shows SEM images of CBR, SBR, and PIB cryogels formed in benzene at $T_{prep} = -18$ °C and at a rubber concentration C_R of 5 % (w/v) [55]. The crosslinker (S_2Cl_2) concentration is 6 and 12 % in the upper and lower panels, respectively. The cryogels derived from CBR and SBR exhibit an aligned porous structure consisting of regular pores with sizes 10^1–10^2 μm, separated by pore walls of 10–20 μm in thickness. Decreasing the concentration of CBR or SBR in the feed further increased the regularity of the porous structure [55]. As indicated in Sect. 4.1, the regularity of the pore structure increases with decreasing freezing rate of the reaction solution, or by conducting the cryogelation reactions under isothermal conditions. The latter facilitates homogeneous nucleation of solvent crystals so that the polymer network formed will exhibit monodisperse pores. In the present case, gelation occurs non-isothermally during the initial cooling period of the reaction solution from 20 °C to −18 °C, which takes place in about 5 min [55]. Since decreasing the polymer concentration C_R also decreases the rate of the crosslinking reactions, the gel point is shifted towards longer reaction times as C_R is decreased, so that gelation occurs isothermally in the apparently frozen system, leading to the formation of more regular pores. In contrast, gel networks formed from PIB exhibit a broad size distribution of irregular pores from micrometer to millimeter sizes. Thus, the use of PIB in the gel preparation destroys the regularity of the porous structure in the organogels.

The variation in the morphologies of the cryogels depends on the type of rubber and originates from the different solvating power of benzene for different types of rubber. For instance, Fig. 24a shows the normalized weight swelling ratio m_{rel} of conventional gels based on PIB, CBR, and SBR in benzene plotted against the swelling temperature [55]. Both CBR and SBR gels exhibit temperature-independent swelling behavior and, thus, benzene is a good solvent for these

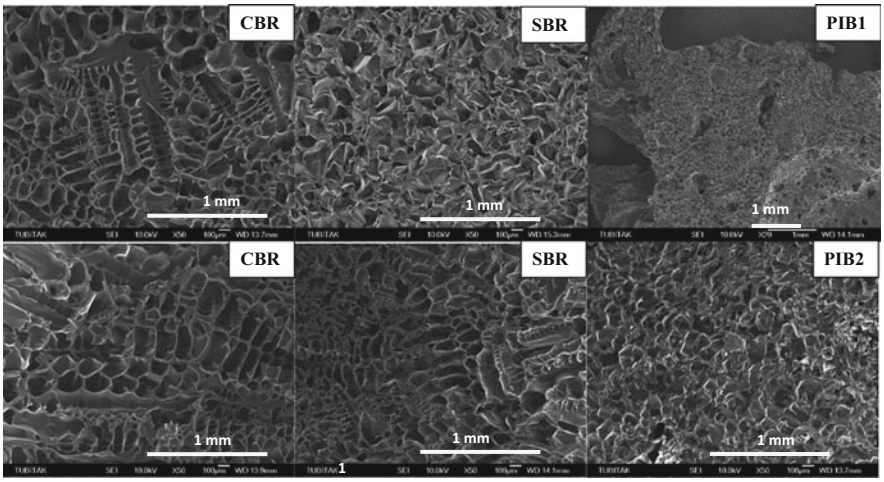

Fig. 23 SEM of the gel networks formed from the various rubbers indicated. C_R =5 %; S_2Cl_2 = 6 % (*upper row*) and 12 % (*bottom row*). The degree of unsaturation of PIB was 1.1 % (PIB1) and 2.3 % (PIB2). (From [55] with permission from Elsevier)

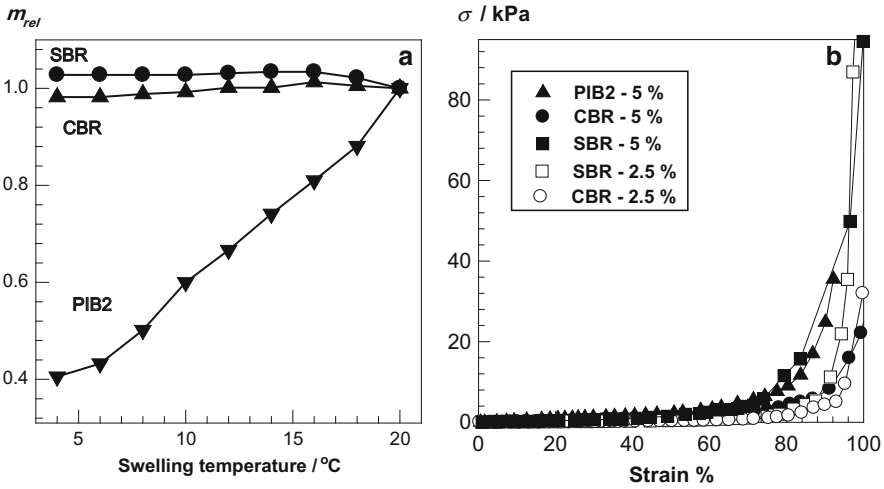

Fig. 24 **(a)** Normalized weight swelling ratio m_{rel} of conventional gels based on SBR, CBR, and PIB2 in benzene shown as a function of the swelling temperature. The gels were prepared at 20 °C in the presence of 12 % S_2Cl_2. **(b)** Typical stress–strain data of rubber cryogels. Types of rubber and the rubber concentration at gel preparation are indicated. (From [55] with permission from Elsevier)

polymers over the whole range of temperatures investigated. This indicates that CBR and SBR remain in the solution during the initial cooling period of the gelation reactions so that only the cryogelation mechanism is responsible for formation of the pores in these networks. However, the swelling capacity of PIB gel strongly depends on the temperature (Fig. 24a); the gel continuously deswells as the temperature is decreased and benzene becomes a poor solvent at low temperatures. Thus, PIB chains are not only expelled from the solution due to cryoconcentration but they also undergo a cooling-induced phase separation to form agglomerates of various sizes. Accordingly, both cryogelation and cooling-induced phase separation mechanisms govern the process of formation of the pores in PIB networks. The formation of millimeter-sized large pores also supports the idea that two mechanisms are operative in the formation of the porous structure in PIB networks.

The total pore volume V_p of the cryogels formed at $C_R = 5$ % (w/v) was 7 ± 0.5 mL/g, independent of the type of rubber and the crosslinker concentration. The value of V_p further increased with decreasing the rubber concentration C_R to 2.5 % (w/v) [55]. Typical stress–strain data of the cryogels derived from PIB, CBR, and SBR are shown in Fig. 24b. None of the rubber cryogels broke, even at a strain of 99.9 %. Sorption tests show that the cryogels are effective sorbents for various pollutants, e.g., crude oil, gasoline, diesel, and olive oil [54, 55, 69]. The sorption rate of all cryogels is very rapid due to their interconnected pore structure and they absorb the pollutants in less than 10–20 min to attain thermodynamic equilibrium. Moreover, PIB gels exhibit the fastest uptake rate for the pollutants, probably due to their large pores formed by phase separation. In Fig. 25a, the maximum sorption capacities of CBR, SBR, and PIB cryogels are compared for various pollutants. SBR or CBR cryogels sorb 35–38 g crude oil or 23–26 g olive oil per gram, as compared to 23 g/g and 9 g/g, respectively, using the PIB gel. We should mention that the widely used oil sorbents based on polypropylene have sorption capacities for both crude oil and olive oil of about 15 g/g [54]. Thus, SBR and CBR gels have sorption capacities about twice that of the commercial oil sorbents. Another point shown in Fig. 25a is that the sorption capacity of the cryogels is highest for crude oil, i.e., for the pollutant with highest viscosity. This implies that, although increased viscosity of the pollutant decreases the rate of sorption, favorable hydrophobic interactions between the crude oil and the hydrophobic polymer dominate the sorption process so that more oil is retained within the rubber gels.

The reusability of rubber cryogels and their continuous sorption capacities were also demonstrated by conducting sorption–squeezing cycles [54, 55]. The cycles were repeated 20 times to obtain the recycling efficiency and continuous extraction capacity of the cryogels. The results are shown in Fig. 26, where the uptake capacity of the gels in each cycle for various pollutants is plotted against the number of sorption–squeezing cycles. The amount of pollutant sorbed in each cycle is almost

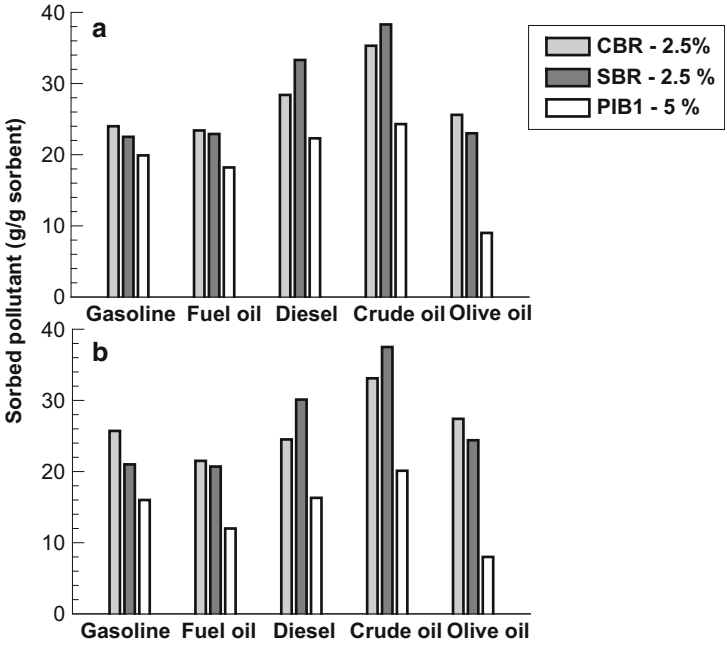

Fig. 25 (**a**) Maximum and (**b**) continuous sorption capacities of the cryogels for various pollutants. Types of rubber and the rubber concentration at gel preparation are indicated. $S_2Cl_2 = 6$ %. (From [55] with permission from Elsevier)

constant for the number of cycles larger than six; for example, it is equal to 37.5 ± 0.1 g crude oil/g and 24.4 ± 0.1 g olive oil/g for SBR gels formed at C_R = 2.5 %. The average of the sorption capacities (i.e., the continuous extraction capacities) of the best sorbents are collected in Fig. 25b. The results clearly demonstrate that the continuous capacity is close to the maximum capacity of gels, indicating high reusability of all cryogels and recoverability of crude oil, petroleum products, and olive oil. Sorption tests conducted using pollutants that spread on the water surface gave similar results as those in Fig. 26 [55]. The fact that 37.5 g crude oil can be recovered by 1 g of SBR gel in one cycle means that about one ton of crude oil can be separated from surface waters by use of 1 kg SBR gel within 25 cycles. Due to the fast responsivity of the cryogel, when put onto sea water, it immediately absorbs crude oil on the water surface. Successive sorption–squeezing cycles can continuously remove crude oil from water and, at the same time, crude oil is recovered.

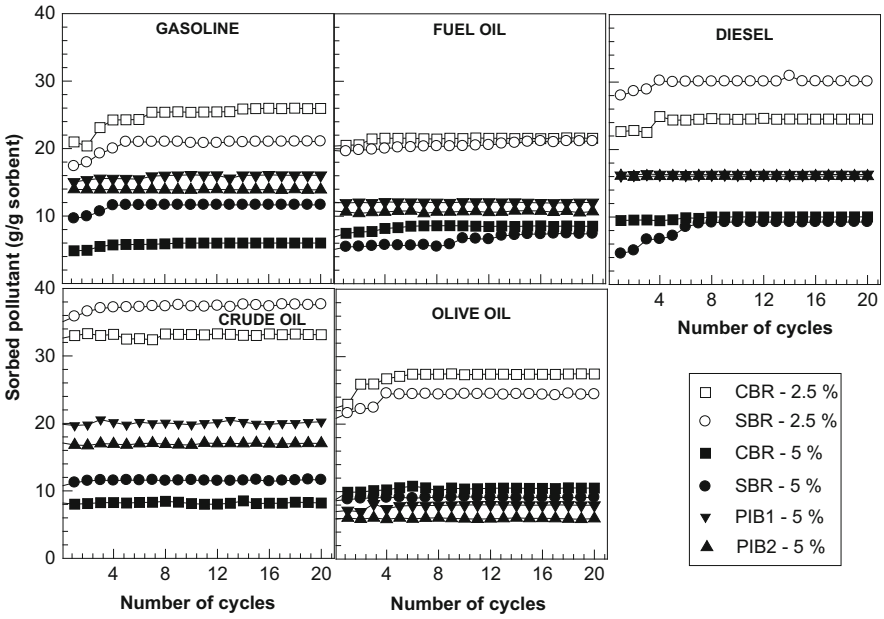

Fig. 26 Continuous extraction capacities of the cryogels for various pollutants as a function of the number of cycles. $S_2Cl_2 = 6$ %. $C_R = 5$ %: PIB1 (*inverted triangle*), PIB2 (*filled triangle*), CBR (*filled square*), SBR (*open circle*). $C_R = 2.5$ %: CBR (*open square*) and SBR (*open circle*). (From [55] with permission from Elsevier)

6 Concluding Remarks

In recent years, strategies for the synthesis of macroporous gels have been continually optimized and the concept of cryogelation has become increasingly important for the synthesis of such smart materials. Cryogelation is a simple strategy that allows the preparation of macroporous gels with high toughness and superfast responsivity. Although discovered over 30 years ago, cryogels have attracted intense attention only in the last 10 years due to their extraordinary properties. Cryogels are very tough gels that can withstandhigh levels of deformation, such as elongation and torsion, and can be squeezed almost completely without any crack propagation. The cryogelation temperature, the freezing rate of the reaction solutions, the type and concentration of the gel precursors, and the solvent are the main synthesis parameters determining the properties of the resultant cryogel. Some novel cryogels presented in this chapter (including DNA, silk fibroin, PAAc, and rubber cryogels) show that cryogelation technology opens new application areas for macroporous materials. Current research in the field of macroporous gels is focused on tailor-made design of the pore structure. The polymerization and/or crosslinking reactions at subzero temperatures that lead to cryogels are multicomponent systems composed of a polymer network, soluble polymers, and low molecular weight

compounds (monomers and solvent) in equilibrium with solvent crystals. All concentrations and properties of the system components change continuously during the cryogelation process. A more complete understanding of this complicated gel formation system is needed in order to improve the structuring of cryogels overall length scales from nanometer to micrometer. Moreover, because the volume swelling ratio of the cryogels and their porosity are inversely coupled, new synthetic approaches are also needed for the preparation of cryogels exhibiting drastic volume changes in response to external stimuli.

Acknowledgement This work was supported by the Scientific and Technical Research Council of Turkey (TUBITAK, TBAG–211 T044) and the Russian Foundation for Basic Research (RFBR, 12-03-91371). O.O. thanks the Turkish Academy of Sciences (TUBA) for the partial support.

References

1. Gerlach G, Arndt KF (2009) Hydrogel sensors and actuators. In: Urban G (ed) Springer series on chemical sensors and biosensors, vol 6. Springer, Berlin
2. Shibayama M, Tanaka T (1993) Adv Polym Sci 109:1
3. Galaev I, Mattiasson B (2008) Smart polymers. Applications in biotechnology and biomedicine, 2nd edn. CRC Press, NY
4. Suzuki M, Hirasa O (1993) Adv Polym Sci 110:241
5. Tanaka T, Fillmore DJ (1979) J Chem Phys 70:1214
6. Gong JP, Katsuyama Y, Kurokawa T, Osada Y (2003) Adv Mater 15:1155
7. Okumura Y, Ito K (2001) Adv Mater 13:485
8. Tuncaboylu DC, Sari M, Oppermann W, Okay O (2011) Macromolecules 44:4997
9. Haraguchi K, Takehisa T (2002) Adv Mater 14:1120
10. Huang T, Xu H, Jiao K, Zhu L, Brown HR, Wang H (2007) Adv Mater 19:1622
11. Okay O (2000) Prog Polym Sci 25:711
12. Seidl J, Malinsky J, Dusek K, Heitz W (1967) Adv Polym Sci 5:113
13. Dusek K (1982) In: Haward RN (ed) Developments in polymerization, vol 3, Applied Science, London, p 143
14. Sayil C, Okay O (2001) Polymer 42:7639
15. Vainerman ES, Lozinsky VI, Rogozhin SV (1981) Colloid Polym Sci 259:1198
16. Lozinsky VI, Vainerman ES, Titova EF, Belavtseva EM, Rogozhin SV (1984) Colloid Polym Sci 262:769
17. Lozinsky VI (2002) Russ Chem Rev 71:489
18. Lozinsky VI, Plieva FM, Galaev IY, Mattiasson B (2002) Bioseparation 10:163
19. Lozinsky VI, Galaev IY, Plieva FM, Savina IN, Jungvid H, Mattiasson B (2003) Trends Biotechnol 21:445
20. Mattiasson B, Kumar A, Galaev IY (2010) Macroporous polymers. Production, properties, and biotechnological/biomedical applications. CRC Press, New York
21. Henderson TMA, Ladewig K, Haylock DN, McLean KM, O'Connor AJ (2013) J Mater Chem B 1:2682
22. Kirsebom H, Mattiasson B (2011) Polym Chem 2:1059
23. Ozmen MM, Dinu MV, Dragan ES, Okay O (2007) J Macromol Sci Part A 44:1195
24. Plieva FM, Karlsson M, Aguilar MR, Gomez D, Mikhalovsky S, Galaev IY (2005) Soft Matter 1:303
25. Plieva F, Huiting X, Galaev IY, Bergenstahl B, Mattiasson B (2006) J Mater Chem 16:4065
26. Dinu MV, Ozmen MM, Dragan ES, Okay O (2007) Polymer 48:195

27. Lozinsky VI, Kalinina EV, Grinberg VY, Grinberg NV, Chupov VV, Plate NA (1997) Polym Sci Ser A 39:1300
28. Kirsebom H, Rata G, Topgaard D, Mattiasson B, Galaev IY (2009) Macromolecules 42:5208
29. Kumar A, Plieva FM, Galaev IY, Mattiasson B (2003) J Immunol Methods 283:185
30. Sun X-L, He W-D, Li J, Li L-Y, Zhang B-Y, Pan T-T (2009) J Polym Sci Part A Polym Chem 47:6863
31. Bilici C, Karayel S, Demir TT, Okay O (2010) J Appl Polym Sci 118:2981
32. Zhang X-Z, Chu C-C (2003) Chem Commun 12:1446
33. Perez P, Plieva F, Gallardo A, Roman JS, Aguilar MR, Morfin I, Ehrburger-Dolle F, Bley F, Mikhalovsky S, Galaev IY, Mattiasson B (2008) Biomacromolecules 9:66
34. Zheng S, Wang T, Liu D, Liu X, Wang C, Tong Z (2013) Polymer 54:1846
35. Andac M, Plieva FM, Denizli A, Galaev IY, Mattiasson B (2008) Macromol Chem Phys 209:577
36. Ozmen MM, Okay O (2005) Polymer 46:8119
37. Petrov P, Petrova E, Tsvetanov CB (2009) Polymer 50:1118
38. Kahveci MU, Beyazkilic Z, Yagci Y (2010) J Polym Sci Part A Polym Chem 48:4989
39. Reichelt S, Abe C, Hainich S, Knolle W, Decker U, Prager A, Konieczny R (2013) Soft Matter 9:2484
40. Sun X-L, He W-D, Pan T-T, Ding Z-L, Zhang Y-J (2010) Polymer 51:110
41. Zhao Q, Sun J, Wu X, Lin Y (2011) Soft Matter 7:4284
42. Lozinsky VI, Vainerman ES, Rogozhin SV (1982) Colloid Polym Sci 260:776
43. Ivanov RV, Lozinsky VI, Noh SK, Han SS, Lyoo WS (2007) J Appl Polym Sci 106:1470
44. Lozinsky VI, Plieva FM (1998) Enzyme Microb Technol 23:227
45. Welzel PB, Grimmer M, Renneberg C, Naujox L, Zschoche S, Freudenberg U, Werner C (2012) Biomacromolecules 13:2349
46. Auriemma F, DeRosa C, Ricciardi R, Lo Celso F, Triolo R, Pipich V (2008) J Phys Chem B 112:816
47. Orakdogen N, Karacan P, Okay O (2011) React Funct Polym 71:782
48. Karacan P, Okay O (2013) React Funct Polym 73:442
49. Karakutuk I, Ak F, Okay O (2012) Biomacromolecules 13:1122
50. Ak F, Oztoprak Z, Karakutuk I, Okay O (2013) Biomacromolecules 14:719
51. Okay O, Durmaz S, Erman B (2000) Macromolecules 33:4822
52. Ceylan D, Okay O (2007) Macromolecules 40:8742
53. Dogu S, Okay O (2008) Polymer 49:4626
54. Ceylan D, Dogu S, Karacik B, Yakan S, Okay OS, Okay O (2009) Environ Sci Technol 43:3846
55. Karakutuk I, Okay O (2010) React Funct Polym 70:585
56. Tuncaboylu DC, Okay O (2010) Langmuir 26:7574
57. Pojanavaraphan T, Liu L, Ceylan D, Okay O, Magaraphan R, Schiraldi DA (2011) Macromolecules 44:923
58. Kirsebom H, Mattiasson B, Galaev IY (2009) Langmuir 25:8462
59. Ozmen MM, Okay O (2008) React Funct Polym 68:1467
60. Lozinsky VI, Vainerman ES, Korotaeva GF, Rogozhin SV (1984) Colloid Polym Sci 262:617
61. Lozinsky VI, Morozova SA, Vainerman ES, Titova EF, Shtil'man MI, Belavtseva EM, Rogozhin SV (1989) Acta Polym 40:8
62. Ivanov RV, Babushkina TA, Lozinsky VI (2005) Polym Sci Ser A 47:791
63. Ozmen MM, Okay O (2006) J Macromol Sci Part A 43:1215
64. Tripathi A, Kumar A (2011) Macromol Biosci 11:22
65. Arvidsson P, Plieva FM, Savina IN, Lozinsky VI, Fexby S, Bulow L, Galaev IY, Mattiasson B (2002) J Chromatogr A 977:27
66. Arvidsson P, Plieva FM, Lozinsky VI, Galaev IY, Mattiasson B (2003) J Chromatogr A 986:275
67. Plieva FM, Andersson J, Galaev IY, Mattiasson B (2004) J Sep Sci 27:828

68. Plieva FM, Savina IN, Deraz S, Andersson J, Galaev IY, Mattiasson B (2004) J Chromatogr B 807:129
69. Tuncaboylu DC, Okay O (2009) Eur Polym J 45:2033
70. Plieva FM, Mattiasson B (2008) Ind Eng Chem Res 47:4131
71. Yun J, Tu C, Lin D-Q, Xu L, Guo Y, Shen S, Zhang S, Yao K, Guan Y-X, Yao S-J (2012) J Chromatogr A 1247:81
72. Yun J, Dafoe JT, Peterson E, Xu L, Yao S-J (2013) J Chromatogr A 1284:148
73. Topuz F, Okay O (2009) React Funct Polym 69:273
74. Yin W, Yates MZ (2008) Langmuir 24:701
75. Gun'ko VM, Savina IN, Mikhalovsky SV (2013) Adv Colloid Int Sci 187–188:1
76. Savina IN, Tomlins PE, Mikhalovsky SV, Galaev IY (2010) Characterization of macroporous gels. In: Mattiasson B, Kumar A, Galaev IY (eds) Macroporous polymers. Production, properties, and biotechnological/biomedical applications. CRC Press, New York, p 211
77. Flory PJ (1953) Principles of polymer chemistry. NY, Cornell University Press, Ithaca
78. Treloar LRG (1975) The physics of rubber elasticity. University Press, Oxford
79. Hertz H (1881) Über die Berührung Fester Elastischer Körper (on the Contact of Elastic Solids). J. Reine und Angewandte Mathematik 92:156. In: Jones DE, Schott GA (eds) (1896) Miscellaneous papers b H. Hertz. Macmillan, London
80. Knaebel A, Rebre SR, Lequeux F (1997) Polym Gels Networks 5:107
81. Briscoe BJ, Liu KK, Williams DR (1998) J Colloid Int Sci 200:256
82. Barquins M, Shanahan MER (1997) Int J Adhes Adhes 17:313
83. Lozinsky VI, Zubov AL, Titova EF (1996) Enzyme Microb Technol 18:561
84. Lu W-M, Tung K-L, Hung S-M, Shiau J-S, Hwang K-J (2001) Powder Techn 116:1
85. Funke W, Okay O, Joos-Muller B (1998) Adv Polym Sci 36:139
86. Oppermann W, Rose S, Rehage G (1985) Br Polym J 17:175
87. Baker JP, Hong LH, Blanch HW, Prausnitz JM (1994) Macromolecules 27:1446
88. Naghash HJ, Okay O (1996) J Appl Polym Sci 60:971
89. Gundogan N, Okay O, Oppermann W (2004) Macromol Chem Phys 205:814
90. Bromberg L, Grosberg AY, Matsuo ES, Suzuki Y, Tanaka T (1997) J Chem Phys 106:2906
91. Wolfe J, Bryant G, Koster KL (2002) Cryo-Lett 23:157
92. Franks F (1986) Cryo-Lett 7:207
93. Watanabe K, Mizoguchi M (2002) Cold Reg Sci Technol 34:103
94. Okay O, Durmaz S (2002) Polymer 43:1215
95. Loo S-L, Krantz WB, Lim T-T, Fane AG, Hu X (2013) Soft Matter 9:224
96. Ceylan D, Ozmen MM, Okay O (2006) J Appl Polym Sci 99:319
97. Okoroafor EU, Newborough M, Highgate D, Augood P (1998) J Phys D Appl Phys 31:3120
98. Patil RD, Mark JE, Apostolov A, Vassileva E, Fakirov S (2000) Eur Polym J 36:1055
99. Zhang H, Cooper AI (2007) Adv Mater 19:1529
100. Zhang H, Edgar D, Murray P, Rak-Raszewska A, Glennon-Alty L, Cooper AI (2008) Adv Funct Mater 18:222
101. Zhang X-Z, Chu C-C (2003) J Mater Chem 13:2457
102. Kirsebom H, Topgaard D, Galaev IY, Mattiasson B (2010) Langmuir 26:16129
103. Lozinsky VI, Zubov AL, Kulakova VK, Titova EF, Rogozhin SV (1992) J Appl Polym 44:1423
104. Lozinsky VI, Bakeeva IV, Presnyak EP, Damshkaln LG, Zubov VP (2007) J Appl Polym Sci 105:2689
105. Lozinsky VI, Savina IN (2002) Colloid J 64:336
106. Podorozhko EA, D'yakonova EA, Kolosova O, Klabukova LF, Lozinsky VI (2012) Colloid J 74:708
107. Dosseh G, Xia Y, Alba-Simionesco C (2003) J Phys Chem B 107:6445
108. Xu J, LaBean TH, Craig SL (2004) In: Ciferri A (ed) Supramolecular polymers, CRC Press, New York, Chapter 12, p 445

109. Bloomfield VA, Crothers DM, Tinoco I (2000) Nucleic acids: structures, properties, and functions. University Science, Sausalito
110. Okay O (2011) J Polym Sci B Polym Phys 49:551
111. Topuz F, Okay O (2008) Macromolecules 41:8847
112. Topuz F, Okay O (2009) Biomacromolecules 10:2652
113. Murakami Y, Maeda M (2005) Biomacromolecules 6:2927
114. Ishizuka N, Hashimoto Y, Matsuo Y, Ijiro K (2006) Colloids Surf A 284–285:440
115. Amiya T, Tanaka T (1987) Macromolecules 20:1162
116. Horkay F, Basser PJ (2004) Biomacromolecules 5:232
117. Costa D, Miguel MG, Lindman B (2007) J Phys Chem B 111:8444
118. Costa D, Miguel MG, Lindman B (2010) Adv Coll Int Sci 158:21
119. Orakdogen N, Erman B, Okay O (2010) Macromolecules 43:1530
120. LePecq J-B, Yot P, Paoletti C (1964) C R Acad Sci 259:1786
121. Waring MJ (1965) J Mol Biol 13:269
122. Pohl FM, Jouin TM, Baehr W, Holbrook JJ (1972) Proc Natl Acad Sci USA 69:3805
123. Celedon A, Wirtz D, Sun S (2010) J Phys Chem B 114:16929
124. Sobell HM, Tsai CC, Jain SC, Gilbert SG (1977) J Mol Biol 114:333
125. Berman HM, Young PR (1981) Annu Rev Biophys Bioeng 10:87
126. Faulhaber K, Granzhan A, Ihmels H, Otto D, Thomas L, Wells S (2011) Photobiol Sci 10:1535
127. Vepari C, Kaplan DL (2007) Prog Polym Sci 32:991
128. Vollrath F, Porter D (2009) Polymer 50:5623
129. Hardy JG, Romer LM, Scheibel TR (2008) Polymer 49:4309
130. Murphy AR, Kaplan DL (2009) J Mater Chem 19:6443
131. Vlierberghe SV, Dubruel P, Schacht E (2011) Biomacromolecules 12:1387
132. Zhou CZ, Confalonieri F, Medina N, Zivanovic Y, Esnault C, Yang T, Jacquet M, Janin J, Duguet M, Perasso R, Li ZG (2000) Nucleic Acids Res 28:2413
133. Sofia S, McCarthy MB, Gronowicz G, Kaplan DL (2001) J Biomed Mater Res 54:139
134. Jin HJ, Fridrikh SV, Rutledge GC, Kaplan DL (2002) Biomacromolecules 3:1233
135. Jin HJ, Kaplan DL (2003) Nature 424:1057
136. Karageorgiou V, Kaplan D (2005) Biomaterials 26:5474
137. Nazarov R, Jin HJ, Kaplan DL (2004) Biomacromolecules 5:718
138. Ki CS, Park SY, Kim HJ, Jung HM, Woo KM, Lee JW, Park YH (2008) Biotechnol Lett 30:405
139. Hutmacher DW (2000) Biomaterials 21:2529
140. Li MZ, Lu SZ, Wu ZY, Yan HJ (2001) J Appl Polym Sci 79:2185
141. Li MZ, Wu ZY, Zhang CS, Lu SZ, Yan HJ, Huang D, Ye HL (2001) J Appl Polym Sci 79:2192
142. Lv Q, Feng QL (2006) J Mater Sci Mater Med 17:1349
143. Liu X, Ma PX (2004) Ann Biomed Eng 32:477
144. Zhang Q, Yan S, Li M (2009) Materials 2:2276
145. Kim UJ, Park J, Kim HJ, Wada M, Kaplan DL (2005) Biomaterials 26:2775
146. Min S, Gao X, Liu L, Tian L, Zhu L, Zhang H, Yao JJ (2009) Biomater Sci 20:1961
147. Chen X, Knight DP, Shao ZZ, Vollrath F (2002) Biochemistry 41:14944
148. Mo C, Holland C, Porter D, Shao Z, Vollrath F (2009) Biomacromolecules 10:2724
149. Kim UJ, Park J, Li C, Jin HJ, Valluzzi R, Kaplan DL (2004) Biomacromolecules 5:786
150. Ayub ZH, Arai M, Hirabayashi K (1993) Biosci Biotech Biochem 57:1910
151. Yoshida R, Takahashi T, Yamaguchi T, Ichijo H (1997) Adv Mater 9:175
152. Luo Y, Epstein IR (1991) J Am Chem Soc 113:1518
153. Rabai G, Orban M, Epstein IR (1990) Acc Chem Res 23:258
154. Yoshida R, Ichijo H, Hakuta T, Yamaguchi T (1995) Macromol Rapid Commun 16:305
155. Crook CJ, Smith A, Jones RAL, Ryan AJ (2002) Phys Chem Chem Phys 4:1367
156. Edblom EC, Luo Y, Orban M, Kustin K, Epstein IR (1989) J Phys Chem 93:2722

157. Ende MTA, Peppas NA (1996) J Appl Polym Sci 59:673
158. National Research Council (2003) Oil in the sea III: inputs, fates, and effects. National Academies Press, Washington, DC
159. Adebajo MO, Frost RL, Kloprogge JT, Carmody O, Kokot S (2003) J Porous Mat 10:159
160. Valderrama C, Gamisans X, Heras FX, Cortina JL, Farran A (2007) React Funct Polym 67:1515
161. Sun X-F, Sun R, Sun J-X (2002) J Agric Food Chem 50:6428
162. Deschamps G, Caruel H, Borredon M-E, Bonnin C, Vignoles C (2003) Environ Sci Technol 37:1013
163. Radetic MM, Jocic DM, Jovancic PM, Petrovic ZL, Thomas HF (2003) Environ Sci Technol 37:1008
164. Wei QF, Mather RR, Fotheringham AF (2005) Bioresour Technol 96:331
165. Carmody O, Frost R, Xi Y, Kokot S (2007) Surf Sci 601:2066
166. Gardon JL (1965) In: Mark HF, Gaylord NG, Bikales NM (eds) Encyclopedia of polymer science and technology. Interscience, New Yok, vol 3, p 833
167. Barton AFM (1991) CRC handbook of solubility parameters and other cohesion parameters, second edition. CRC Press, New York
168. Stirna U, Cabulis U, Beverte I (2008) J Cell Plastics 44:139